Quantification and consequences of glacier volume loss on meltwater fluxes and organic matter since 1971, Edgeøya, Svalbard.

Elise van Winden
3472116

Supervisors
Dr. Walter Immerzeel
Dr. Jorien Vonk

Universiteit Utrecht

Quantification and consequences of glacier volume loss on meltwater fluxes and organic matter since 1971, Edgeøya, Svalbard.

Abstract

Due to increasing temperatures in the Arctic, the 36,000 km^2 of glacier ice on Svalbard is decreasing rapidly. Consequently, this will affect meltwater fluxes and organic matter release, which influences the marine ecosystem. The organic matter in glaciers has its source by biological production, wind-blown dust and soil/bedrock erosion and can be degraded to the greenhouse gas CO_2 when released in rivers and ocean. The aim of this research project is to quantify the changes in glacier volumes and its meltwater fluxes over the last 40 years and to characterize the organic matter in these glacial meltwater rivers at Svalbard.

Ice volume estimates have been conducted for the years 1971, 2004 and 2014 by volume/area-scaling and a GIS approach based on Weertman's sliding law. The ice area, based on remote sensing and topographic maps, is used to initialize and calibrate a cryospheric hydrology model to model the consequence of ice loss on meltwater flow. During the Dutch Scientific Expedition Edgeøya Spitsbergen (SEES) water samples of 13 of these glacial meltwater rivers have been collected. These samples are analyzed for stable isotopes in meltwater (δ^2H and $\delta^{18}O$) and organic matter ($\delta^{13}C$), which elucidate the source of the water (glacial or snow) and organic matter (terrestrial or autochthonous), respectively. We also determine the total amount of organic carbon (dissolved and particulate) transport, as well as its molecular characteristics and its bioavailability.

Results show over 40% ice volume loss since 1971 and all ice will be gone prior to 2100. The base flow and number of glacier melt days are slightly increasing from 1971 onwards. This suggests that glacier melt per unit area is increasing with time to counteract glacier area decline. Whether the total annual discharge is already declining due to area loss or if this is going to happen in the near future is unclear, since the modeled data is not verified with field data. In meltwater rivers we measured 0.5-5*10^3 mg/L of total suspended matter, containing 0.80-1.5% organic carbon. These values are low, which can be explained by the thin and poorly developed soils in this high-Arctic setting. Organic matter is mainly from terrestrial sources (-24‰ - -29‰). The source of the river water was mainly from glacier water. We estimate that the additional ice mass loss leads to an increase of 1.5Mton/yr organic carbon loading, important for near coastal zone ecosystems. These results help to assess the degree of sensitivity of these Arctic river systems for a warming future.

Contents

List of figures

List of tables

1. Introduction

Climate is warming (IPCC, 2013) and this results in a reduction of glacier volumes (e.g.(Hagen et al., 1991)) and increase in permafrost thawing (e.g.(Spencer et al., 2015; Westermann et al., 2011)) worldwide, but at faster rate in the polar region (IPCC, 2013). Glacier decline might result in more river discharge (Hagen et al., 2003a) resulting in a higher fresh water flux to the oceans where it will have its influence on sea life and ocean circulation (Fellman et al., 2010; Hood et al., 2009). Furthermore, the flux of organic matter (OM) in glaciers released by melting, and the amount picked up on the way by permafrost/soil erosion is also likely to change (Spencer et al., 2014a), due to increased permafrost thaw. The OM in Svalbard glaciers and rivers is hardly studied, and unknown in amount and bioavailability. The link between climate change induced glacier melt since the 1970's, its consequent changes in river discharge and OM flux, and the OM from permafrost thawing and soil erosion at Svalbard and, more specifically at Edgeøya, is the base for this study. The aim of this research project is to quantify the changes in glacier volumes and its meltwater fluxes over the last 40 years and to characterize the organic matter in the glacial meltwater rivers at Svalbard. A change in organic matter flux to the ocean is fundamentally important for marine life, since it is the basis of their foodweb.

Glaciers

For most glaciers in the world, the latest increase in glacier volume was during the little ice age, which occurred between the 15th and 19th century (Svendsen and Mangerud, 1997). Since then glaciers have been retreating worldwide, and due to human-induced climate change glacier retreat now occurs at even faster rates (Nuth et al., 2010).

Many researchers have investigated ice volume decline in Svalbard, all come with results of net negative mass balance for Svalbard and Edgeøya. The mass balance of a glacier is the result of ice incoming (e.g. precipitation, avalanche, flux) minus outgoing (melt, wind redistribution, flux, sublimation) at any location on the glacier or ice cap, where the specific net mass balance being the result of the entire glacier or ice cap over a year. At Edgeøya from 1970/71-2002 values of -0.50 m water equivalent (w.e.)y^{-1} and up to -1.00±0.0 m y^{-1} are reported (James et al., 2012; Kääb, 2008; Nuth et al., 2010). Similar values for all Svalbard glaciers have been reported by several authors (Braithwaite and Raper, 2007; James et al., 2012; Malecki, 2013; Sobota, 2007). These values are in sharp contrast with reported values of -0.12±0.1m, -0.12±0.03m, -0.19m w.e. y^{-1} (Bamber et al., 2005; Hagen et al., 2003b; Moholdt et al., 2010, respectively). Most of the variability is due to the large differences between Svalbard regions; For instance, thickening at northeast Svalbard ice caps is measured which neutralizes negative mass balance in other regions slightly. Despite the high variability, all report negative mass balances. Due to present-day warming enhanced glacier melt has been recorded: from -0.5 to -0.7m w.e. y^{-1} (1970/71-2002) (Kääb, 2008); from -0.15 to -0.69m w.e. y^{-1} from 1936 to 2005 (Kohler et al., 2007); from -0.52±0.09 to 0.76±0.1m m y^{-1} from prior to after the 1990's (James et al., 2012), resulting in more mass loss. Enhanced glacier melt is caused by the negative mass balance and results in an upward shift of the Equilibrium line altitude (ELA) between the accumulation and ablation zone at the glacier, which has an albedo change as result (Oerlemans et al., 2009).

Hydrology

Glacier volume loss influences the meltwater flux from glacier to ocean, which can either increase due to an increase in mass loss, or decrease when the total ice area declines. Fresh meltwater can influence circulation and local ecosystem of the oceans and coastal zones (Hagen et al., 2003a) and results in sea level rise, so an increase or decrease in meltwater flux is fundamentally important to investigate. Moreover, Svalbard's glacier can contribute with 17-20mm of sea level rise (SLR) when all glacier melt completely (Martin-Espanol, 2013), this is only a minor contribution of al cryospheric input to SLR, compared to ice melt at the Greenland and Antarctic ice cap, but still an important contribution. Meltwater rivers fluctuate highly annually, as shown by (Radić and Hock, 2014) who modeled 40% variation in annual glacial discharge (worldwide). In Svalbard 30% annual discharge variation is measured (Hagen et al., 2003a) with higher variation in the last 10 years than in the 1990's (Nowak and Hodson, 2013).

Future projections show rising temperatures and prolong the glacier melt season (Nowak and Hodson, 2013) and show an increase of +54% in discharge in Svalbard in the mid-21st century and a decline to -10% of the initial values at 2100, mainly explained by the negative mass balance of glaciers (Bliss et al., 2014). This increase followed by a decrease in discharge is also found in other glaciated regions as Alaska and the Himalayas (Fellman et al., 2010; Hood et al., 2009; Immerzeel et al., 2012, 2013). The precise moment on which the decline in discharge will start, may, however, be very different by region (Bliss et al., 2014). Rising temperatures in arctic regions, also deepen the active layer in permafrost, creating an storage, but also a source of melt water (Nowak and Hodson, 2013). The future projections are very sensitive to future temperature and precipitation changes and slight offsets may result in different projections. That precipitation is important is explained by many researchers; not only does an increase in precipitation result in more glacier accumulation, or might it counteract the decline in discharge by decrease in glacier area, it also influences monthly discharges by more and heavier precipitation events (Hagen et al., 2003a; Immerzeel et al., 2012, 2013; Nowak and Hodson, 2013; Owczarek et al., 2014). Not only are hydrological changes dependent on the net mass balance of the glacier and therefore on future temperature and precipitation rates, but also on ice area, size of the drainage basin (Hagen et al., 2003a), thermal regime of the glacier (cold or warm based), as well as the spatial and temporal variation in the hydraulic properties of the glaciers surface (Rutter et al., 2011)

Organic Matter (OM)

There are several sources of organic matter (OM) in glaciers: (1) Englacial autotrophic microbial life (bacteria, viruses and algae) fixates carbon from the atmosphere in OM. Most of this OM is coupled to debris in cryoconite holes as particulate organic carbon (POC), but also partly (10%) as dissolved organic carbon (DOC) (Anesio et al., 2009). On average about 0.11 dissolved mg C/L DOC is present in glacial ice around the world (Priscu and Christner 2004). Besides the production by microbial life, (2) aerosols with soil OM and combusted carbon together with (3) subglacial debris entrainment contribute to the glacial carbon pool. This OM is transported as POC and DOC in meltwater and added to the OC released by soil and permafrost erosion on the way down before entering the ocean.

The glacial OM has been measured as highly bioavailable (Hood et al., 2009; Spencer et al., 2014a) as it is easily utilized by microbes, and is more bioavailable than OM from wetlands in study sites in Alaska (Fellman et al., 2010). The bioavailability is dependent on age and molecular composition

(Mann et al., 2015; Spencer et al., 2015; Vonk et al., 2013), and glaciers are expected to have older DOC than enclosed wetlands (Spencer et al., 2014a). At present 13% of the annual flux of glacier-derived DOC entering the ocean is the result of glacier mass loss, which is expected to accelerate (Hood et al., 2015). Even though the measured DOC values (in Alaska) are low (0.18-0.53 mg C/L), researchers agree that the labile OC flux is important for coastal zone life's metabolism and sensitive to seasonal and future runoff changes (Fellman et al., 2010; Hood et al., 2009; Kim et al., 2011; Spencer et al., 2014a).

Research questions

In this study, the quantity, lability and source of organic matter with the glacier loss rate and consequently, meltwater fluctuations, as reference for Svalbard will be investigated. So, how much and how fast does glacier mass loss occur (1), what is its influence on the meltwater flux (2) and what is the amount, bioavailability and source of the OC that is released and transported by these glaciers and meltwater rivers before entering the ecosystem-sensitive coastal zone (3)? For research questions (1) and (2), an area of 1000km^2 in northwest Edgeøya has been chosen. OC research has been conducted after fieldwork in South and East Svalbard with special focus on Edgeøya.

(1) Glacier volume loss has been quantified by the volume-area scaling and a modelling effort in which ice thickness is a factor of slope and equilibrium shear stress. Areas have been measured with the use of satellite images in GIS and derived from the Randolf Glacier Inventory (RGI). The results are compared with volumes calculated by Huss, which is based on flow dynamics, inverted from the surface topography (Huss and Farinotti, 2012).

(2) Meltwater flux is modeled in a pcRaster model based on (Immerzeel et al., 2012) in which discharge is a factor of glacier and snow melt, a digital elevation model (DEM) together with precipitation and temperature data. The model is calibrated for the glacier area extent as it is in 2014 based on satellite images.

(3) During the Dutch Scientific Expedition Edgeøya Spitsbergen in August 2015 (SEES) water samples of 13 glacial meltwater rivers have been collected. These samples were analyzed for stable isotopes in meltwater (δD and $\delta^{18}O$) and organic matter ($\delta^{13}C$), which will elucidate the source of the water (glacial or snow) and organic matter (terrestrial or autochthonous), respectively. We will also determine the total amount of transport of organic carbon (dissolved and particulate), as well as its molecular characteristics and its bioavailability.

Combining the results will give a more complete overview of the source, quality and export of OM in Svalbard glacier systems, an important study to enhance knowledge about future climate change impact on these changing areas.

2. Study area

Glacier volume loss calculations and meltwater modelling has been done for ice caps on NE Edgeøya, one of the eastern islands of Svalbard (figure 1). Organic matter research from these glaciers and in these rivers has been done on the island Spitsbergen, Edgeøya and Barentsøya (figure 2).

Edgeøya (77.0N/22.3E) is an 5074km^2 island covered by approximately 2102 km^2 ice (Dowdeswell and Bamber, 1995), and located in the Barents Sea. Deglaciation started 10 ky BP and since then the island has experience glacioeustatic uplift, leaving quaternary marine deposits in the lower parts of the valleys. The upper part of the valleys and the plateaus shaped by former ice caps, consist of Triassic flat lying sedimentary rock (Moller et al., 1995). It's on these plateaus where smaller and larger icecaps are situated with glacier tongues into and shaping the valleys.

Four of these ice caps are studied for their volume loss: Langjokulen + Kvitisen, Blaisen, Bergfonna and Raundalsfonna. All are flat lying ice caps, with a maximum altitude of 560m, having low ice movement and more than one glacier tongue. Only one surge has been reported from one of these glaciers, near Kvitisen in 1965 (Dowdeswell and Bamber, 1995), but all glaciers show terminus retreat since the little ice age. The ELA is considered to be at approximately 300m (Hagen et al., 2003b), and moving upwards with increasing air temperatures. The meltwater from these ice caps runs into 11 different valleys.

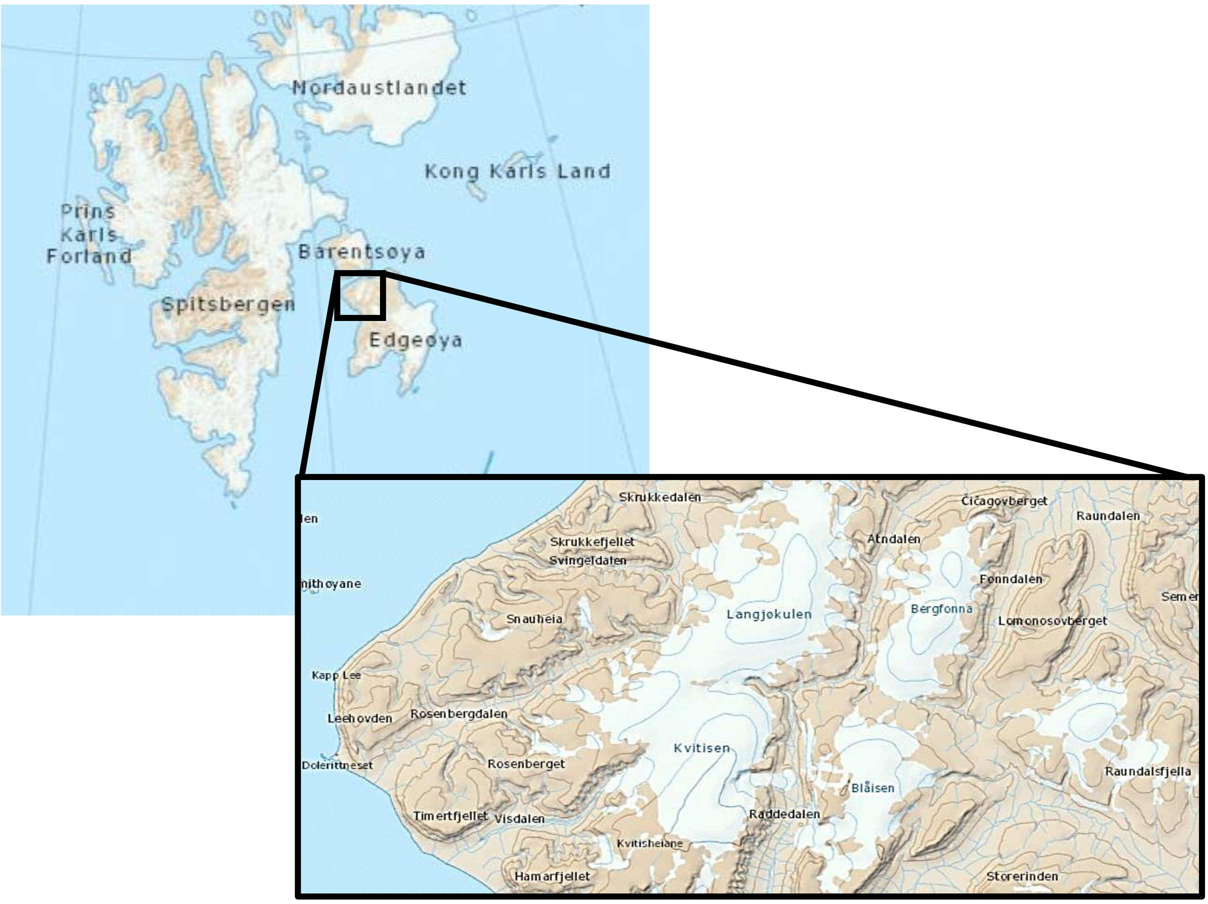

Figure 1; Svalbard and its Edgeøya, glacier volume research areas are located in the red box in the map on the right side

The sample points for OM research are taken at different locations around Spitsbergen, Barentsøya and Edgeøya. The distance from sampling point to the glacier front differs per location, as does the discharge. Three river valleys have been sampled: Rosenbergdalen, Plurdalen and Kvalpyntfonna. At Rosenbergdalen, more than one sample has been taken to investigate the variability downstream.

Temperatures are on average below 0ºC with summer temperatures reaching occasionally 15ºC and winter temperatures can be as low as -40ºC. Precipitation is around 200 mm/yr. Both temperature and precipitation data has been taken from the weather station at Longyearbyen airport. At Edgeøya only temperature has been measured for a few years, which show slightly colder temperatures then at Longyearbyen Airport. There is no precipitation record available from Edgeøya.

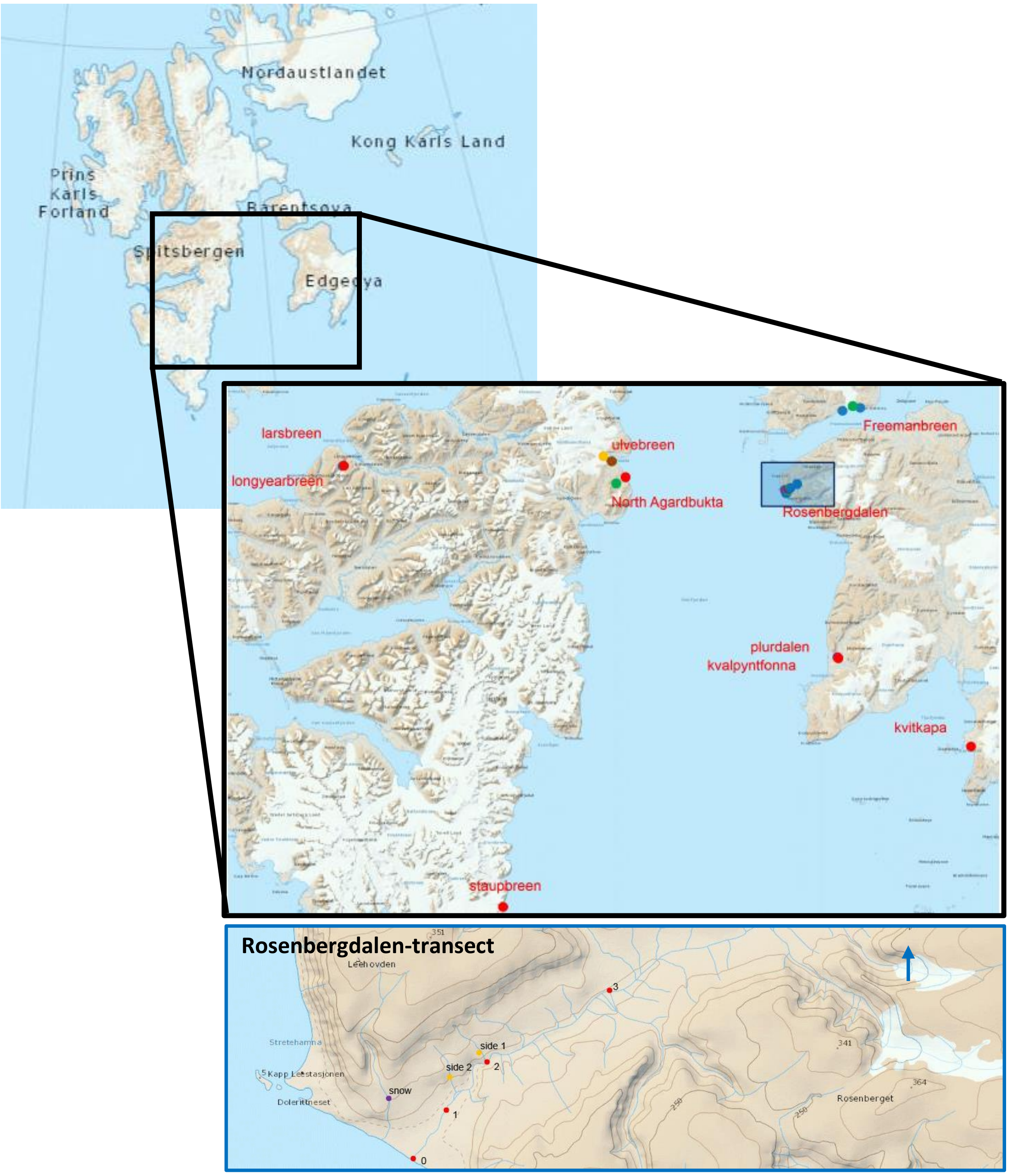

Figure 2; Sample locations for OM research with on the left the sample location as taken in Rosendalen

3. Methods

3.1 Volume determination

To estimate the volume loss of the glaciers at Edgeøya, different methods have been compared: (1) The mathematical method of the Volume-Area scaling (e.g. Bahr et al., 1997), applied by several researchers and used worldwide, which determines the glacier and ice cap volume (V) based on its surface area (S).

(2) The GIS-method uses Weertmans sliding law (Weertman, 1957) with a full DEM in a GIS-based environment, in which the initial thicknes (H) of the ice bodies is calculated based on the equilibrium shear stress. By multiplying the average thickness of a polygon with the surface area, the volume is calculated. Both methods are used to calculate the volume of the ice bodies for the years 1971, 2003-2004 and 2014.

(3) The Huss-method (Huss and Farinotti, 2012) is a physically based approach based on ice flow dynamics inverted from the surface geometry. Volume and ice thickness data has been received personally to compare with the other ice-volume deriving methods.

3.1.1 Volume-Area scaling

The surface-volume ratio as described in Bahr et al. (1997), Grinsted (2013), Jiyang Chen and Ohmura (1990), Macheret and Zhuravlev (1982), Martín-Español et al. (2015), Radić and Hock (2010), Van De Wal and Wild (2001), assumes a relationship between the glacier's surface area and its volume. The ratio between surface area (S) and volume (V) is defined as:

$$V \approx c\, S^{\gamma} \qquad (1)$$

with constant values for the proportionality constant c, and exponent γ based on glacier type. Different studies find different values for parameters c and γ. Bahr et al. (1997) describes the physical background of exponent γ which is based on four variables that determine the volume and surface area of a glacier: width (q), slope (r), side drag (f), mass balance (m) together with Glen's flow law constant (n). These variables determine the γ as:

$$\gamma = 1 + \frac{1+m+n(f+r)}{(q+1)(n+2)} \qquad (2)$$

Bahr et al. (1997) uses previous glacier volume measurements to find the best values for the variables and finds $\gamma = 1.375$ for glaciers and , $\gamma = 1.25$ for ice caps. Others (see table 1) find slightly different values for often a specific region; as they are based on volume measurements by GPR, sea level fluctuations and field-based measurements. With the formulas as listed in table 1, the volumes of all ice caps and glaciers of northwestern Edgeøya are calculated.

The surface area (S) for the years 1971, 2004 and 2014 is derived by GIS software based on the GLIMS dataset provided by the Norsk Polar Institute (NPI) (www.npolar.no, cryoclim-map) and a Landsat 8 satellite image, respectively. The chosen glacier outlines by the NPI do not separate the ice caps from its outlet glaciers, which is needed for some V/A-scaling methods (table 1). Therefore an arbitrary distinction based on the slope of the polygon and the area-perimeter ratio has been made: assumed is that glaciers have a steeper slope and a larger area-perimeter ratio compared to ice caps. The area outlines, and the distinction between glaciers (regular characters) and ice caps (bold characters) are shown in figure 3. The derived surface areas are then used to calculate the ice volume.

*Table 1; Volume-Area scaling formulas as found in literature. Most methods are based on an inventory of glaciers as the Randalf Glacier Inventory (RGI) and the World Glacier Inventory (WGI). *Van De Wal and Wild (2001) based their constant (c) on an expected sea level rise of 0.5m if all glaciers would melt.*

	Source	Ice body	Formula	Comments and specific locations
A B	Bahr et al. (1997)	Glaciers Glaciers	$V = 0.0276A^{1.36}$ $V = 0.0276A^{1.375}$	Based on 144 glaciers Based on physics
C1 C2 D	Grinsted (2013)	Glaciers Ice caps $A \leq 25km^2$	$V = 0.0433A^{1.29}$ $V = 0.0432A^{1.23}$ $V = 0.0435A^{1.23}$	Based on RGI glaciers Based on RGI ice caps Based on WGI
E F	Martín-Español et al. (2015)	Glaciers Glaciers	$V = 0.0343A^{1.329}$ $V = 0.0454A^{1.264}$	Method a Method b based on 60 Svalbard gl.
G1 G2	Radić and Hock (2010)	Glaciers Ice caps	$V = 0.0365A^{1.375}$ $V = 0.0538A^{1.25}$	Based on WGI
H	Macheret and Zhuravlev (1982)	Glaciers	$V = 0.0597A^{1.12}$	Based on Svalbard gl.
I	Van De Wal and Wild (2001)	Glaciers	$V = 0.0213A^{1.375}$	Based on sea level*
J	Chen and Ohmura (1990)	Glaciers	$V = 0.0285A^{1.375}$	Based on alpine gl.

Figure 3; Glacier outlines in yellow (1971), red (2004) and blue (2014) as produced by the NPI and this study. Bold numbers correspond to icecaps, regular numbers to glaciers, distinction based on perimeter/area-ratio and the polygon's slope.

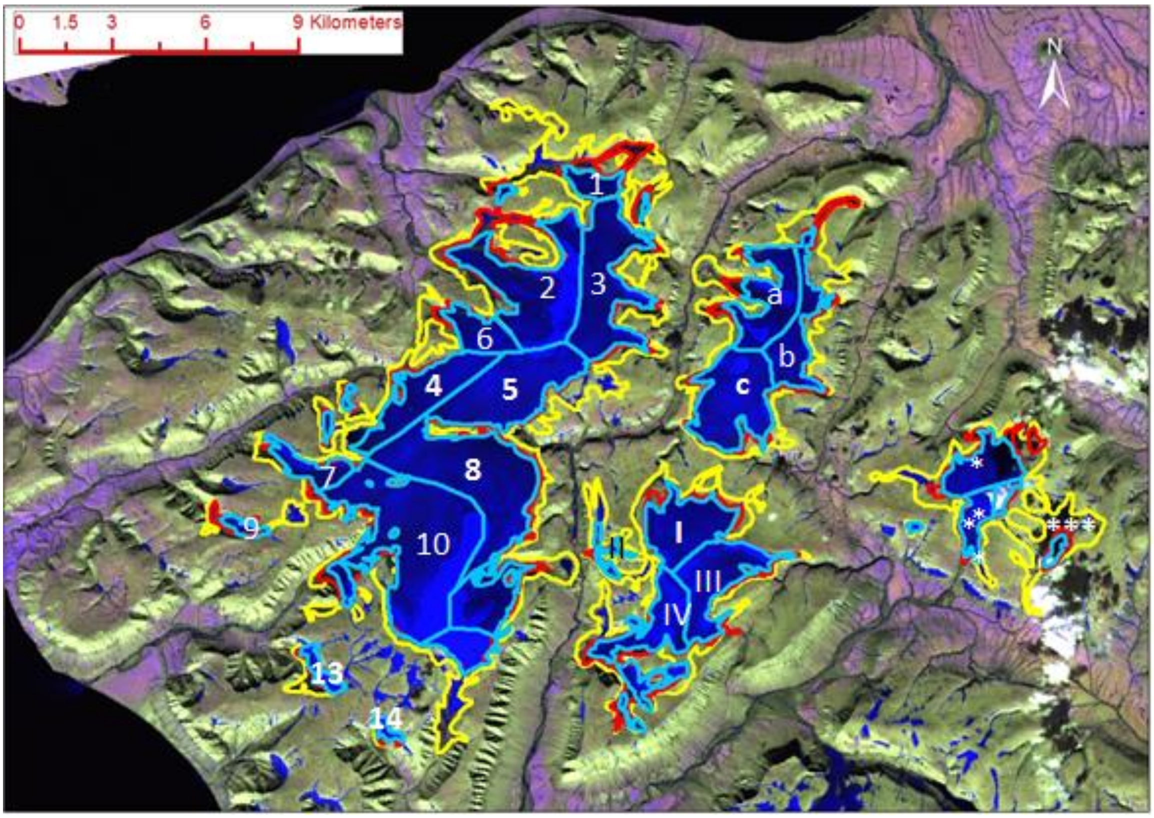

*Numbers 1-14 Langjokulen and Kvitisen, a-c from Bergfonna and I-IV from Blaisen, *-*** for raundalsfjella. The map is a landsat 8 satellite false color image with bands in 4, 5, 1 combination.*

3.1.2 GIS-method

The volume loss of glaciers has been modelled in GIS-software based on Weertman's sliding law (Weerman 1957, Fowler 1957). This law is based on the relation between basal sliding and basal shear stress: when the basal ice is above 0°C, a film of water between the ice and the bed allows slip. A thicker ice package increases the pressure of the ice on the bed, allowing the pressure melting point to increase, causing a water film which causes the basal shear stress to overcome the friction at the bed. This results in a faster flow of ice and thinning of the ice. The reverse is true as well, thinning of the ice decreases the ice pressure, decreasing the pressure melting point and the ice freezes to the bed and starts moving slower. So, on a certain slope only a maximum thickness of ice can occur, in other words it will move to lower areas when the thickness and therefore the basal shear stress, is exceeded. This interconnection between pressure, stress and thickness results in the following formula (Immerzeel et al., 2012):

$$H = \frac{\tau_0}{\rho\ g\ sin\beta} \qquad (3)$$

with the ice thickness (H), the basal shear stress (τ_0) in Pa, the slope (β) in °, the ice density (ρ) in kg/m^3, and gravity (g) in m/s^2. Together with a DEM (Norsk Polar Institute, 2014) and the glacier outlines as used in previous method, the volume loss has been modelled in GIS by using Weertman's sliding law.

Beforehand, preprocessing is needed to make the data appropriate for volume modelling: In Weertman's sliding law, the slope used is the bedrock slope. Here the surface slope is used as a proxy and since the DEM is based on the topography map with a contour interval of 100m height. Smoothing is necessary of 240m per grid cell, since this is the average distance between the contour intervals. The slope is minimum set at 1°, this to prevent the thickness to be unlimited. The ice density is 916.7 kg/m^3. The equilibrium shear stress is equal to the average basal shear stress along a central flow line and is calculated as in (Haeberli, 2005) by the formula:

$$\tau_0(kpa) = 0.5 + 159.8\Delta h - 43.5(\Delta h)^2 \qquad (4)$$

With Δh as the difference in altitude in km.
At last the volume of the glaciers and ice caps is calculated combining the surface area and grid cell calculated ice thickness as:

$$V = S * H \qquad (5)$$

These alterations have been done for every polygon to determine the volume and rate of volume change for the years 1971, 2004 and 2014.

3.1.3 Huss&Farinotti method

The Huss&Farinotti method is used in this thesis to compare results with the V/A-scaling and GIS-method. Their data have been received personally and have been used in Huss and Farinotti (2012). Shortly, as explained in their paper, this method is a physically based approach for calculating the glaciers' thickness and it's volume. The ice thickness is derived from inverting the surface topography based on the flow dynamics as in Glen's flow law ($\varepsilon = A\tau^n$). This combines the mass balance distribution with the ice flux and accounts for glaciers' characteristics as surface geometry, local climate and the distribution of the ice thickness corrected for basal sliding and the thermal regime of the glacier. This method holds the assumption of a minimal slope of 6°, and all parameters encompass some uncertainty. The ice thickness output is handled in grid cells and the volume is derived by multiplying the grid cell's calculated ice thickness with its surface area.

3.2 Modelling glacier extent, volume and its meltwater flux

3.2.1 General approach

The ice volume and meltwater flux of the Edgeøya's ice caps have been modelled in a grid-based dynamic model (PcRaster,(Karssenberg et al., 2001)) as previously done in Immerzeel et al. (2012). Every day's ice thickness is calculated by the use of temperature (T) and precipitation (P) datasets and ice flow (F) in each cell on a DEM. The climate data have been taken from meteorological stations located at Svalbard, and ice flow is one of the key processes and assumed to be basal sliding only as by Weertman's sliding law. The initial ice thickness and extent as from satellite images from 1971 is the basis for modelling the volume and extent of 2014, giving a 43 year simulation period, which is calibrated by trial and error. After the volume of glacier loss has been calculated, based on the keyprocesses of ablation, mass balance and ice fluxes, the hydrology of NW Edgeøya is modelled, similar as in (Immerzeel et al., 2012; Shea et al., 2015). The total discharge is the sum of the glacier meltwater discharge, snow melt, precipitation and groundwater fluxes minus the water stored in the ground and evaporation. The discharges are visualized in hydrographs for a better understanding of daily, seasonal and decadal variation of the hydrology in this area.

3.2.2 Datasets used

Precipitation

No precipitation data is available from Edgeøya, and therefore taken from Svalbard Airport. Precipitation is low during the year, and is made visible in figure 4. For the first four years of the dataset, the precipitation data is from Longyearbyen city. Here the precipitation is similar to the Airport location with an offset of 0.2 mm in two years. Assumed is that only snow contributes to glacier growth, and precipitation falls as snow at temperatures ≤ 0 °C. No precipitation correction is used with altitude, the precipitation form (snow, rain) is corrected with the temperature lapse rate.

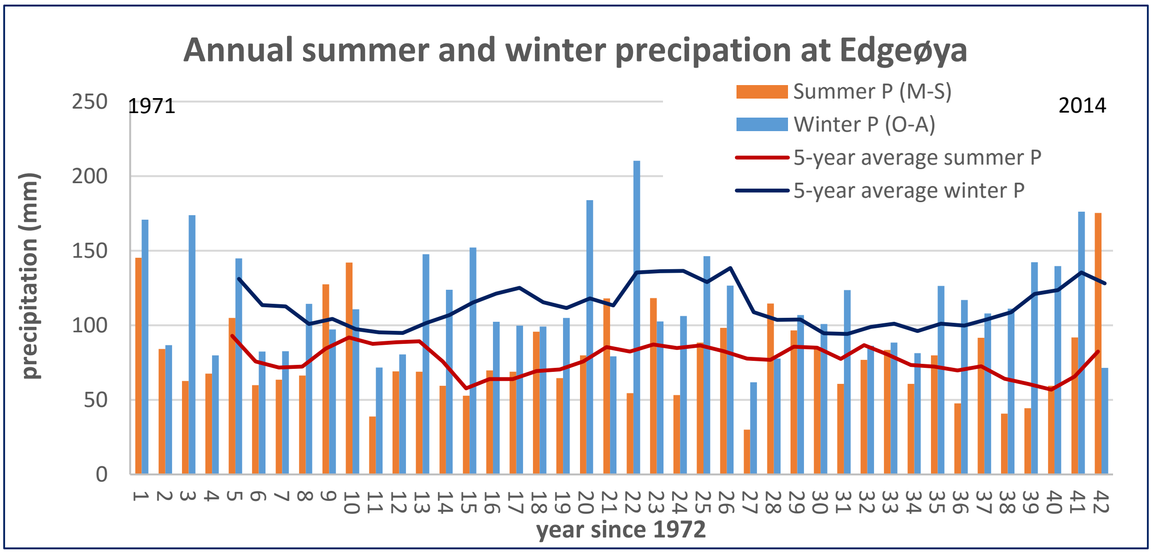

Figure 4; Precipitation data at Longyearbyen, we assume it is similar at Edgeøya.

Temperature

There is no long-term weather monitoring on Edgeøya, but there are several weather station on Svalbard. There is one at Kapp Heuglin working from 2005 to 2007. For this study the weather data from Longyearbyen Airport is taken from 1975 to 2014. The overlapping years with the weather station at Edgeøya are compared with a scatterplot (figure 5). Since temperatures are usually colder at Edgeøya, the temperature at Longyearbyen Airport has been corrected for Edgeøya temperatures. Since we need T going back to 1971, the weather station data of Longyearbyen has been used for the first 4 years, and the same method as above described has been used. For Edgeøya two approaches are taken: linear and polynomial correction, the latter causes higher off sets for colder temperatures, therefor the linear fit has been chosen. Temperature decreases with 5.5 degrees per km height for saturated air and up to 10 degrees for dry air as it depends on adiabatic process. Since temperatures at Svalbard are mostly very low, the air has often high relative humidity but low specific humidity, resulting in low temperature lapse rate values. Temperature profile of Edgeøya is shown in figure 6.

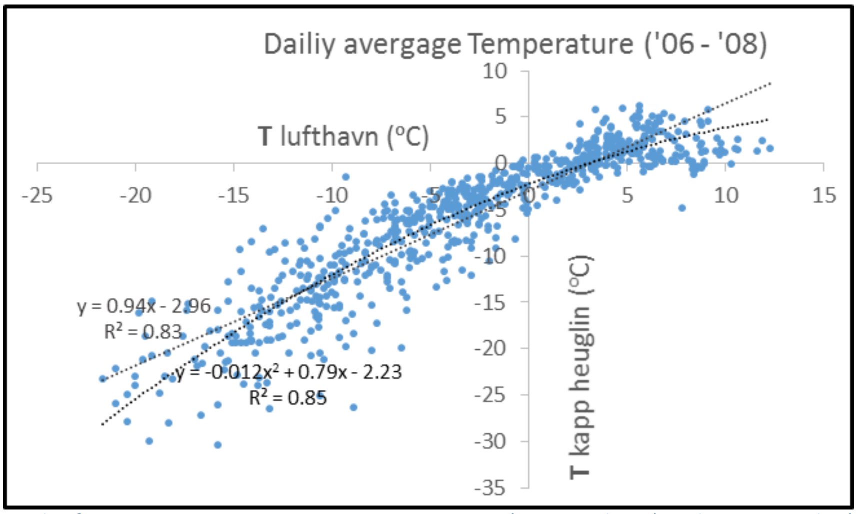

Figure 5; Scatterplot from temperature measurements at Airport (Longyearbyen) and Kapp Heuglin (Edgeøya). Dotted lines are linear and polynomial trend lines to show the correlation between the two sites.

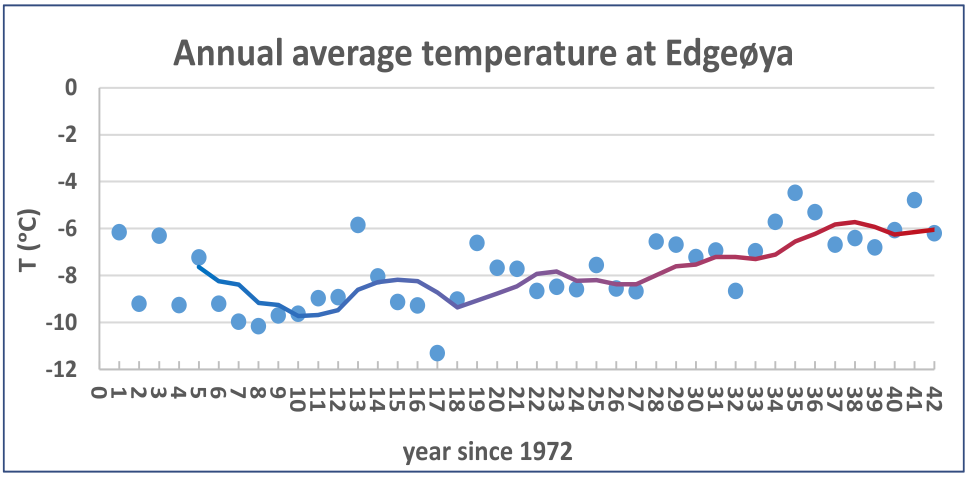

Figure 6; Annual average temperature at Longyearbyen airport and corrected by the linear approach to get the temperature profile as it is at Egeøya. Trendline is the average of 5 year of average temperature.

3.2.3 Key processes

Mass balance

The glacier dynamics are based on the mass balance per grid cell and changes are calculated at daily time steps. The mass balance is added to the ice thickness of the previous day, and is the sum of the net flux (F_{in}-F_{out}) of ice by basal sliding, the accumulation by precipitation in the form of snow (P), and the ablation (A) based on daily temperature:

$$B = (F_{in} + P) - (F_{out} + A) \qquad (6)$$

Therefore this is a simple positive degree day model that assumes all precipitation fallen at t < 0°C accumulates as ice and every day with t > 0°C results in glacier melt. Below, the variables are specified including their role in the model.

Ablation

Ablation is the loss of ice due to melting (including evaporation, sublimation) and calving. In the research area, calving is not occurring and therefore neglected. Melt occurs when energy received by the glacier exceeds its energy loss. Glaciers receive energy from short- and longwave radiation, sensible and latent heat fluxes, glacier's ice temperature changes and (warmer) precipitation. These factors have not been measured in the research area, therefore ablation (A) is assumed to be based on the temperature of the atmosphere when $T < 0^{o}C$ and corrected with a degree day factor (DDF).

$$A = T_{>0} * DDF \qquad (7)$$

The degree day factor is dependent on albedo and the energy balance components and is therefore different per specific region and varies with time. For example, snow has a high albedo, reflecting shortwave radiation strongly and has therefore lower DDF values than ice; and in cases of a low sensible heat flux, the DDF is high. For Svalbard not many studies have been done to estimate the DDF. The most referred one is to (Schytt, 1964), who calculated a DDF of 13.8 mm/°C for Nordaustlanded, which is very high compared to values in other parts of the world. The DDF is also corrected for the aspect with:

$$DDF_a = DDF(1 - C * \cos(a)) \qquad (8)$$

with *a* being the aspect and *C* a correction factor (Konz, 2007, (Immerzeel et al., 2012)).

Ice fluxes

Movement of ice from one cell to another in the model is based on basal sliding as described by Weertman (1957) and neglects deformational flow. In the model a more extensive sliding law is used as in a previous method: Basal sliding dependent on the ice thickness and therefore the pressure melting point at the glaciers bed, is combined with basal ice creep called regelation. Basal sliding occurs when the basal shear stress (τ_b) is larger than the equilibrium shear stress (τ_0). Of which the equilibrium shear stress, as calculated in GIS in the previous method, is used in the model and the basal shear stress, dependent on ice thickness (9), is combined with regelation (10):

$$\tau_b = \rho\, g\, H\, sin(\beta) \qquad (9)$$

$$\tau_b = \vartheta^2 R\, u^{\frac{2}{n+1}} \qquad (10)$$

With ϑ as bedrock roughness, R material roughness both influence how smooth the surface is over which the glacier slide. The velocity is u and n is Glen's flow number (Glen, 1955). Combining the two results in:

$$\vartheta^2 R\, u^{\frac{2}{n+1}} = \rho\, g\, H\, sin(\beta) \qquad (11)$$

Sliding occurs when $\tau_b > \tau_0$, therefore the velocity (u) is:

$$u^{\frac{2}{n+1}} = \frac{\rho\, g\, H\, sin(\beta) - \tau_0}{\vartheta^2 R} \qquad (12)$$

Glens number n is assumed to be 3, resulting in:

$$u = \left(\frac{\rho\, g\, H\, sin(\beta) - \tau_0}{\vartheta^2 R}\right)^2 \qquad (13)$$

So, glacier movement in each cell is modelled as function of slope, ice thickness and assumed bed rock roughness. The outgoing ice flux at each time step is determined by glacier velocity and estimated ice thickness and distributed to lower positioned cells based on the slope. Besides the in and out flux from ice between cells, input from external cells is possible by avalanches as well. Due to the low snowfall, and low slope profiles of the ice caps, avalanches will have minor influence on the ice thickness.

Hydrology

When the glacier part is calibrated, the hydrology part is added in the model. The total discharge (Qtot) is the sum of surface runoff (Qsurf), snow meltwater (Qsnow), glacier meltwater (Qglac) and groundwater fluxes (Qgw). Water is received by precipitation and the melt of ice and snow by ablation and lost by evaporation. With the help of GIS, outlet points at the rivers are drawn and used in the model as locations from which the discharge is presented. The drainage areas connected to each outlet point is derived from pcRastercalc, and its area together with its glaciated area is calculated. The discharge is made visible in hydrographs to show potential runoff changes with increased glacier melt.

The glacier and snow melt leads to surface runoff and groundwater flow. Glacier and snow runoff is calculated as a fraction of the ablation modelled in previous section, and is corrected for refreezing and glacier water storage. Together with the precipitation, the meltwater infiltrates the soil, limited by the retention parameter (S) which is based on the curve number (SCS USDA, 1972). The maximum soil moisture content is set at 0.0375m and based on Osterkamp and Burn (2003), assumed is a silty soil with an active layer depth of 25cm and a water content of 15%. When the maximum soil moisture content is reached it is recharged to the groundwater and excess is drained as surface runoff.

The calculated runoff is corrected by a recession coefficient to correct for any water flux, which is added to the next time step. The recession coefficient for surface runoff (kx) is calculated as and based on Kane et al. (1998)

$$q_t = q_0 * kx \qquad (13)$$

$$kx = e^{\frac{-t}{t^*}} \qquad (14)$$

$$t^* = 33.5 * A^{0.166} \qquad (15)$$

With q_t and q_0 as runoff at timestep t and initial runoff, respectively, and A the basin area (km^2). For an area of 20 km^2, this results in $kx = 0.98201$, used as the initial value in the model. The modelled groundwater and surface runoff, together with snow and glacier melt forms the total meltwater flux (Qm).

In the drainage area, part of the water at the surface is lost due to evapotranspiration. The potential evapotranspiration is derived by the Hargreaves equation:

$$ET = 0.0023 * 0.408 * R * (T_{mean} + 17.8) * \sqrt{T_{max} - T_{min}} \quad (16)$$

$$R = 37.586 * d_{earth-sun} * (\omega * sin\varphi * sin\delta + cos\varphi * cos\delta * sin\omega) \quad (17)$$

With $d_{earth-sun}$ the distance from earth to sun given per day at location of interest, ω the sunset hour angle, δ is the solar declination and φ the latitude (78°N or 1.36rad) (www.civil.uwaterloo.ca). Since the calculated ET is an overestimation, it needs to be corrected by the temperature reduction coefficient (C):

$$C = 0.035 * (100 - h)^{\frac{1}{3}} \quad \text{for h} > 54\% \quad (18)$$

$$C = 0.125 \quad \text{for h} < 54\% \quad (19)$$

The relative humidity (h) is taken from the Kapp Heuglin station Edgeøya (www.weatherandclimate.info) and is on average 85%, this results in a temperature reduction coefficient of 0.086. The evapotranspiration is influenced by the vegetation and therefore corrected by the crop factor (Kc) to calculate the actual evapotranspiration (Eta) (www.fao.org). Chosen is a low factor (0.2), since vegetation on Edgeøya is comparable to young seedlings in size and not continuously wet. The Eta is used to calculate the loss of ice, snow and discharge to the atmosphere.

3.3 Organic matter; preparation and measurements

Samples of 20 meltwater streams and englacial ice were collected during fieldwork at Edgeøya (Svalbard) and was part of the Dutch Scientific research Expedition Edgeøya Svalbard (SEES) carried out onboard the Ortelius, a former Russian scientific ice breaker, in August 2015. The samples have been analyzed for total suspended matter (TSM), dissolved and particulate OC (DOC, POC), stable carbon and water isotopes (δ^{13}C-POC, δ^{2}H, δ^{18}O), bioavailability, and molecular composition. Water was collected in pre-rinsed 1L bottles and was filtered within 24 hours on 47-mm pre-combusted (450°C , 4h) glass microfiber filters (0.7µm). Filtered waters were subsampled into 5, 40 and 250 mL vials for water isotopes, DOC and molecular composition analysis respectively. After filtering, the samples were frozen (filters, molecular composition analysis), kept at 4°C (water isotopes) or at room temperature of 20°C (DOC) and all kept in the dark and returned to the lab in the USA and NL.

3.3.1 TSM, POC, ^{13}C-POC

Filters were weighed prior and after filtering, with the change being the total suspended matter amount filtered and then standardized to mg per liter. Prior to measuring the percentage organic carbon (%OC) and its ^{13}C composition, the filters have been in a desiccator for at least 24h for acid-fumigation which removes the potential inorganic carbon on the filter. The OC on the filter is combusted and the mass of the combustion products are collected, using an elemental analyzer (Fisons Instruments NA1500), resulting in a percentage loss of the filtered material (Van Soelen et al., 2014). This is multiplied by the TSM mass to calculate the absolute mass of OC and then it is standardized to mg/L. The mass ratio of $^{13}C/^{12}C$ of burned carbon is measured by a mass spectrometer (an EA-IRMS, Thermos Deltaplus) at the geochemistry lab of Utrecht University, the Netherlands. The result is expressed in delta notation ($\delta^{13}C$) with respect to the Vienna Peedee Belemnite (VPDB) standard. The standard deviation is <0.35‰ based on international (Graphite quartzite standard NAXOS) and internal (Nicotinamide) reference samples (Van Soelen et al., 2014).

3.3.2 DOC and bioavailability

For the degradability of the organic carbon measurements, an incubation has been set up with $t = 0, 2, 7, 14, 28$ days directly (within 5h) after water sampling and filtering (Fellman et al., 2010). Samples were acidified with concentrated HCl to pH 2 at each timestep to stop degradation. DOC was measured by a Shimadzu TOC V-CSH at Florida State University as described in (Stubbins and Dittmar, 2012). The DOC data are reported as the mean of three replicate injections, for which the standard deviation is <2% and standardized to mg/L. The initial DOC value is measured at $t = 0$, and the rate of carbon degradation is determined by the change from $t = 0$ to $t = 14$ days.

3.3.3 Molecular composition analysis

The DOM in ice and river water is measured by fluorescence spectroscopy and in a Fourier Transform Ion Cyclotron Resonance Mass Spectrometer (FTICR-MS). Fluorescence spectroscopy measures the fluorescence occurring when an excited electron emits its excess energy when returning to its ground state, here with a Jobin Horiba Aqualog. The excitation and emission wavelengths differ for molecules with different biogeochemical characteristics. The wavelength-specific characterization is visualized in excitation-emission plots (EEMS) and together with FT-ICRMS data visualized in a principle compound analysis (PCA) to find covariance. The FTICR-MS detects the motion of an ion in a stable magnetic field, which is dependent on the ion's cyclonic frequency, radius, velocity and energy (mass). Different kind of atoms in the organic molecules can be identified, as well as the ratios between the atomic compounds investigated (O/H, C/H) (Marshall et al., 1998). Samples have been measured at Florida State University with the method described in (Mosher et al., 2015; Spencer et al., 2014b).

3.3.4 Water isotopes

Water samples have been analyzed for its isotopic composition (δD and $\delta^{18}O$, with respect to VSMOW) at NIOZ, the Netherlands, with a Liquid Water Isotope Analyzer (LWIA-45-EP). This is an off axis mass spectrometer, standardized by internal (LGR 3, 5) and external (GISP, SLAP) derived reference samples. During cold periods, the ice is formed from precipitation with lower $\delta^{18}O$ values, compared to present day. This is the effect of decline in evaporation and an earlier rain out of heavier isotopes, since the atmosphere can hold less water vapor at lower temperatures. Therefore the isotopic composition in meltwater river samples, reveals the source: (old) glacier ice or (young) rain. Seven end member samples have been taken in the field: five from glacier ice, two from precipitation. With the isotopic signature of these end members, than the %glacier-derived water can be calculated for the river samples.

The samples are plotted together with the Global Meteorological Water Line (GMWL) and the Local Meteorological Water Line (LMWL) to elucidate the slope between the δD and $\delta^{18}O$ correlation (as in Kendall and McDonell, 1998). The slope is dependent on evaporation and refreezing, basin morphology, source changes and mixing ((Turner et al., 2010; Yde et al., 2012; Yi et al., 2012)). To reveal if water phase transitions have fractionated the isotopic composition in the water samples, the D-excess is plotted against δD together with the LMWL as done in (Yde et al., 2012).

4. Results

4.1 Volume changes

Volumes for all four ice bodies (Langjokulen & Kvitisen, Blaisen, Raundalsfjella and Bergfonna) have been calculated for the years 1971, 2004 and 2014 by Volume/Area-scaling and by using the Weertmans' sliding law on a grid-based model in GIS. The results of these different approaches are described below and are compared with a third method: the Huss&Farinotti method.

4.1.1 Volume/Area scaling

The volume of the four ice bodies, as in figure 3, has been derived by volume area scaling for 1971, 2004, 2014. Since all methods are based on different assumptions, and some apply for glaciers and others for ice caps, the average volume (Vavg) is calculated as the average of methods C2, D and G2 for icecaps and as the average of methods B, C1, E, F, G1, H, I and J for glaciers. Two research groups have a method for both glaciers and icecaps: method D (Grinsted, 2013) and method G (Radić and Hock, 2010) have been calculated for this area separately as V_D and V_G respectively. All volumes derived by volume/area scaling are shown in table 2.

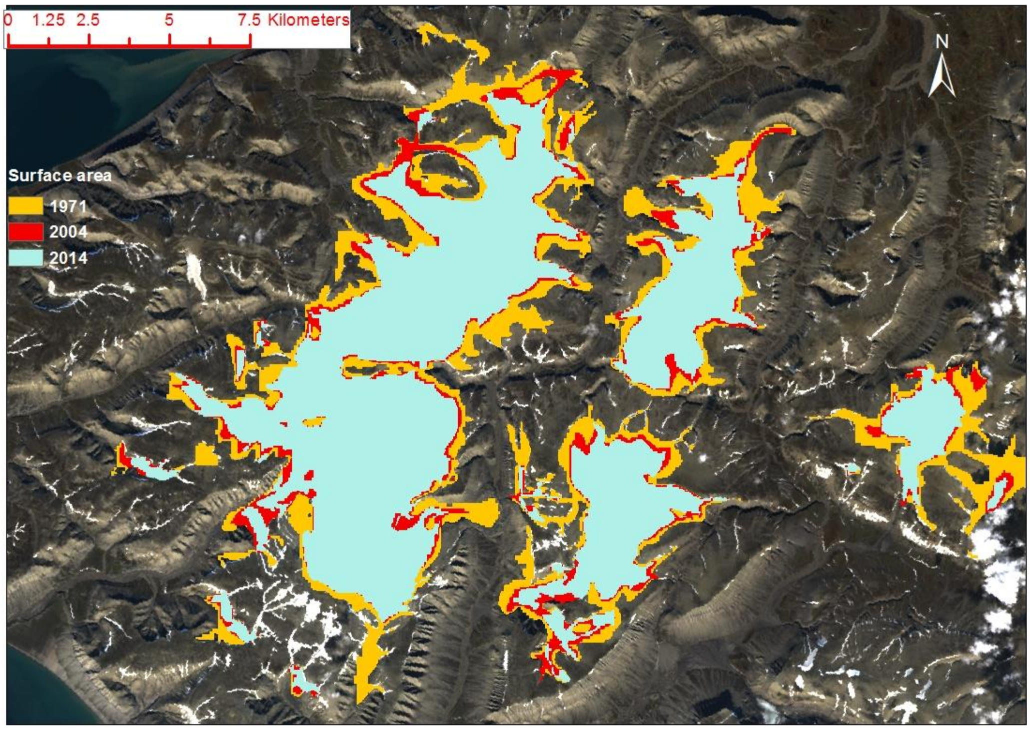

Figure 7; Surface outline of the icecaps and glacier in northwestern Edgeøya for 1971 (yellow), 2004 (red) and 2014 (blue). The map is a landsat 8 satellite natural color image with bands in 1, 2, 3 combination.

Every ice body has lost a large part of their area and volume, as made visible in figure 7. The areas area taken from the WGI, and report a loss of 69km^2 in 43 years, this is a 40% ice area loss. The surface area declines decreases with time, with 1.7km^2/yr from 1971-2004 and 1.4km^2/yr for 2004-2014 and with more loss for smaller ice caps (76% for Raundalsfonna) than larger ice caps (33% for Langjokulen&Kvitisen). In 43 years, Langjokulen & Kvitisen, the largest ice cap in the study area, has lost 37.6±0.6 % of its volume; Bergfonna, Blaisen and Raundalsfjella, all smaller in size, have decreased by respectively 48.1±0.2 %, 44.8±0.2 and 68.0±0.2 % in volume (figure 8). Moreover, this area has lost 43.4±0.6% of its volume (5.5km^3 of original 12.7km^3, in (just) 43 years. The rate of average volume decline in km^3/y decreases slightly from 0.14 for the period 1971-2004 to 0.11 for 2004-2014.

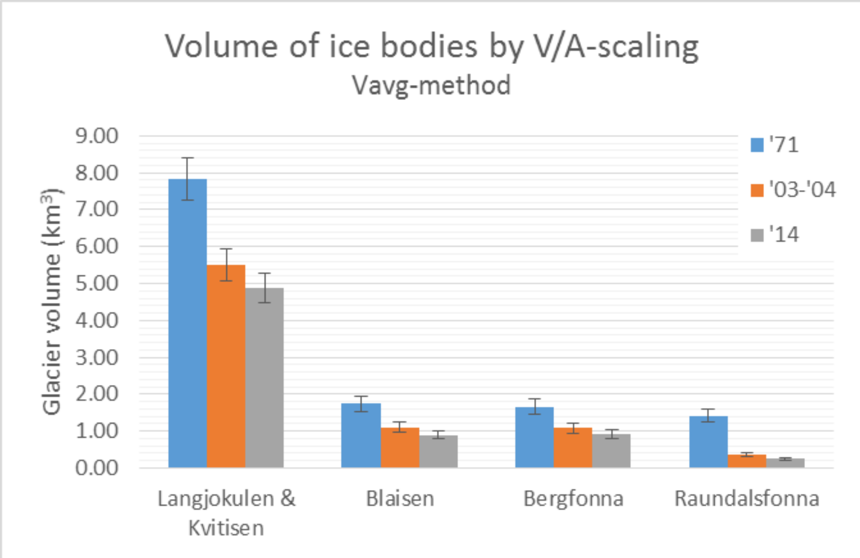

Figure 8; Ice body volumes for 1971, 2004 and 2014 as calculated by volume/area-scaling. The average volume is used, in which glacier and ice caps are distinguished by slope and perimeter/area-ratio as in figure 4.

Table 2; Surface areas (S) in km² and ice body volumes (Vx) in km³ for the years 1971, 2004 and 2014 per ice body as calculated by V/A-scaling. All V/A methods are described in table 1: for ice caps methods C2, D, G2 are used and for glaciers the methods B, C1, E, F, G1, H, I, J. The V_{avg} is the cumulative average volume per ice body with the distinction between glacier and ice cap as in figure 3.

	Glaciers									**Ice caps**			**Glacier & Ice cap**				S (km²)
1971	V_A	V_B	V_{C1}	V_E	V_F	V_{G1}	V_H	V_I	V_J	V_{C2}	V_D	V_{G2}	V_G	V_C	$\mathbf{V_{AVG}}$	V_{SD}	
Langjokulen & Kvitisen	6.6	6.8	8.8	7.6	8.6	9.0	8.1	5.3	7.1	7.6	7.6	9.9	9.4	8.4	**7.8**	0.6	103
Blaisen	1.4	1.5	2.0	1.7	1.9	2.0	1.9	1.1	1.5	1.7	1.7	2.2	2.0	1.9	**1.7**	0.2	26
Bergfonna	1.4	1.4	1.9	1.6	1.9	1.9	1.7	1.1	1.5	1.6	1.7	2.1	2.0	1.8	**1.7**	0.2	24
Raundalsfonna	1.2	1.2	1.6	1.4	1.6	1.6	1.5	0.9	1.3	1.4	1.4	1.8	1.7	1.6	**1.4**	0.2	21
total volume (km^3)	**10.6**	**11.0**	**14.2**	**12.3**	**14.0**	**14.5**	**13.3**	**8.5**	**11.3**	**12.4**	**12.5**	**16.1**	**15.0**	**13.6**	**12.7**	0.7	**173**
2004																	
Langjokulen & Kvitisen	4.6	4.7	6.1	5.3	6.1	6.3	5.9	3.7	4.7	5.4	5.4	7.0	6.5	5.9	**5.5**	0.45	76
Blaisen	0.9	0.9	1.2	1.1	1.3	1.2	1.3	0.7	0.9	1.1	1.1	1.5	1.3	1.2	**1.1**	0.13	18
Bergfonna	0.9	0.9	1.2	1.0	1.2	1.2	1.2	0.7	0.9	1.1	1.1	1.4	1.2	1.1	**1.1**	0.13	17
Raundalsfonna	0.3	0.3	0.4	0.3	0.4	0.4	0.5	0.2	0.3	0.4	0.4	0.5	0.4	0.4	**0.4**	0.05	7
total volume (km3)	**6.6**	**6.8**	**9.0**	**7.7**	**9.0**	**9.0**	**8.8**	**5.3**	**6.8**	**8.0**	**8.0**	**10.3**	**9.5**	**8.6**	**8.0**	0.48	**118**
Reduction since 1971 (%)	37.5	37.7	36.6	37.1	36.2	37.7	33.6	37.7	39.9	35.7	35.7	36.0	37.0	36.5	**36.4**	0.8	32
Annual reduction (km^3/yr)	0.12	0.13	0.16	0.14	0.15	0.17	0.14	0.10	0.14	0.13	0.13	0.18	0.17	0.15	**0.14**		1.7
2014																	
langjokulen & Kvitisen	4.0	4.2	5.5	4.7	5.4	5.5	5.3	3.2	4.2	4.8	4.8	6.2	5.8	5.2	**4.9**	0.4	69
Blaisen	0.7	0.7	1.0	0.9	1.0	1.0	1.1	0.6	0.7	0.9	0.9	1.2	1.0	1.0	**0.9**	0.1	15
Bergfonna	0.7	0.7	1.0	0.9	1.0	1.0	1.0	0.6	0.7	0.9	0.9	1.2	1.1	1.0	**0.9**	0.1	15
Raundalsfonna	0.2	0.2	0.3	0.2	0.3	0.3	0.3	0.2	0.2	0.3	0.3	0.4	0.3	0.3	**0.3**	0.0	5
total volume (km3)	**5.7**	**5.9**	**7.8**	**6.6**	**7.7**	**7.7**	**7.7**	**4.5**	**5.8**	**6.9**	**7.0**	**8.9**	**8.2**	**7.5**	**7.0**	**0.4**	**104**
Reduction since 1971 (%)	46.3	46.5	45.2	45.8	44.8	46.5	41.8	46.5	48.4	44.2	44.2	44.5	45.7	45.2	**45.0**	0.6	40
Annual reduction (km^3/yr)	0.09	0.10	0.12	0.11	0.12	0.13	0.11	0.07	0.10	0.11	0.11	0.14	0.13	0.12	**0.11**		1.4

4.1.2 Modelling ice body volumes in GIS

The initial thickness is dependent on the basal shear stress (τ_0) at the flow line, calculated for every polygon (figure 9). Since ice thickness decreases over time, the basal shear stress and slope (figure 10) needs to be calculated for all time steps. Together with the gravity and ice density constants, the initial thicknesses and the change in ice thickness from 1971 to 2014 (figure 11) are modelled. The volume per ice body per time step is calculated by multiplying the initial thickness with the surface area, results are shown in figure 12 and table 3.

Decrease in area and volume is in the same order as with the V/A-scaling method: Langjokulen & Kvitisen has lost 39.7±3.5 % of its volume. Bergfonna, Blaisen and Raundalsfjella, have decreased by respectively 41.4±1.0 %, 47.9±0.6 % and 73.8±0.3 % in volume. Moreover, the NE ice caps of Edgøya has lost 42.6±3.1% of its volume. The rate of decline of ice volume is from 1971-2004 in the same range as for V/A-scaling: 0.13 km^3/yr; but the present day decline rate is larger: 0.22km^3/yr.

4.1.3 Modelling ice body volumes by Huss&Farinotti's method

Ice body volumes for the year 2004 have been calculated by the Huss&Farinotti method (done by M. Huss) and are shown in table 4. The volumes are smaller than volumes derived by the GIS method and most V/A-scaling methods. The volumes are comparable to the ones calculated by (Martín-Español et al., 2015) which based his V/A-scaling formula on 60 Svalbard glaciers.

Table 3; Surface areas (S) in km² and ice body volumes (Vx in km³ for the years 1971, 2004 and 2014 per ice body as calculated by GIS.

1971	S	V	SD
	(km^2)	(km^3)	
Langjokulen & kvitisen	101.4	**10.89**	2.97
Blaisen	23.8	**1.88**	0.85
Bergfonna	22.5	**1.52**	0.53
Raundalsfonna	12.7	**0.82**	0.32
Total	160	**15.10**	3.15
2004			
Langjokulen & Kvitisen	74.3	**8.14**	2.30
Blaisen	17.0	**1.39**	0.61
Bergfonna	16.1	**1.03**	0.35
Raundalsfonna	6.4	**0.26**	0.11
Total	114	**10.82**	2.41
Reduction since 1971 (%)	29.1	28.4	3.96
Annual reduction (km^3/yr)	1.41	0.13	
2014			
Langjokulen & Kvitisen	67.1	**6.56**	1.80
Blaisen	14.2	**1.10**	0.46
Bergfonna	14.0	**0.79**	0.26
Raundalsfonna	5.2	**0.21**	0.09
Total	100	**8.67**	1.88
Reduction since 1971 (%)	37.4	42.6	3.05
Annual reduction (km^3/yr)	1.33	0.22	

Table 4; Volume and surface area as calculated by Huss-method.

2004	S (km^2)	V (km^3)	SD (±12%)
Langjokulen & Kvitisen	76.1	5.55	0.67
Blaisen	17.7	1.03	0.12
Bergfonna	16.7	0.95	0.11
Raundalsfonna	7.0	0.34	0.04
total volume (km3)	117.4	7.87	0.69

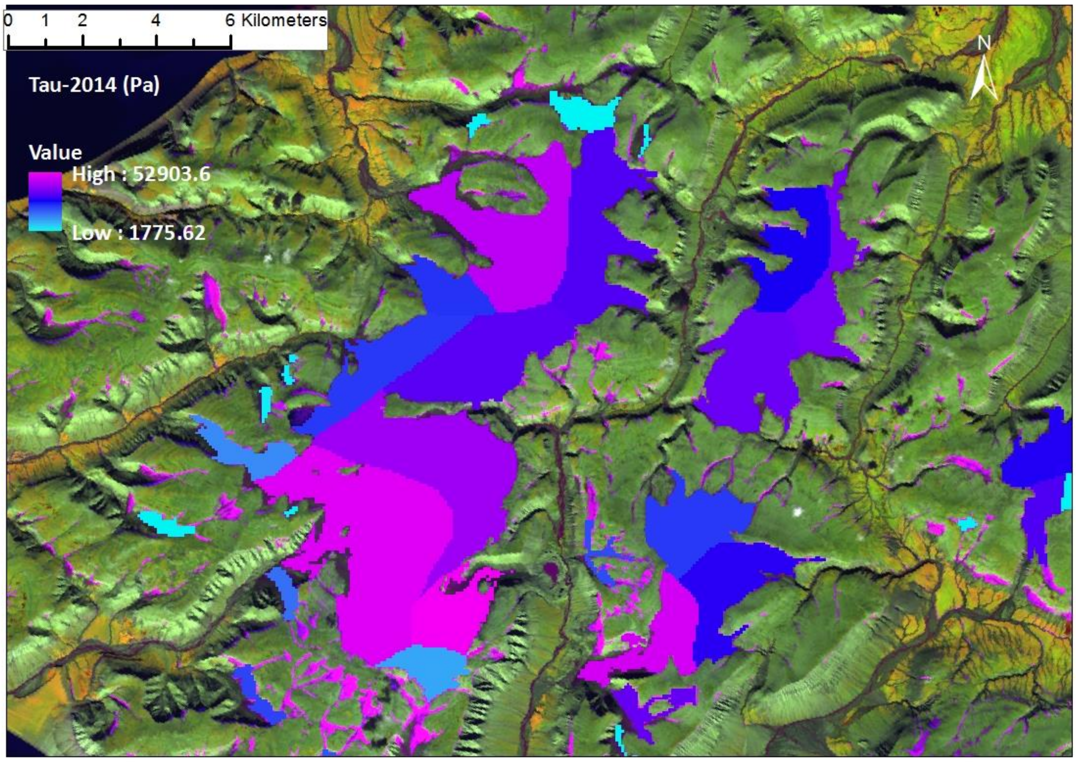

Figure 9; Map of the basal shear stress at the flowline as calculated in (Haeberli, 2005), depending on the altitude range of each glacier. False color satellite image from landsat 8, band colors 4, 5, 1.

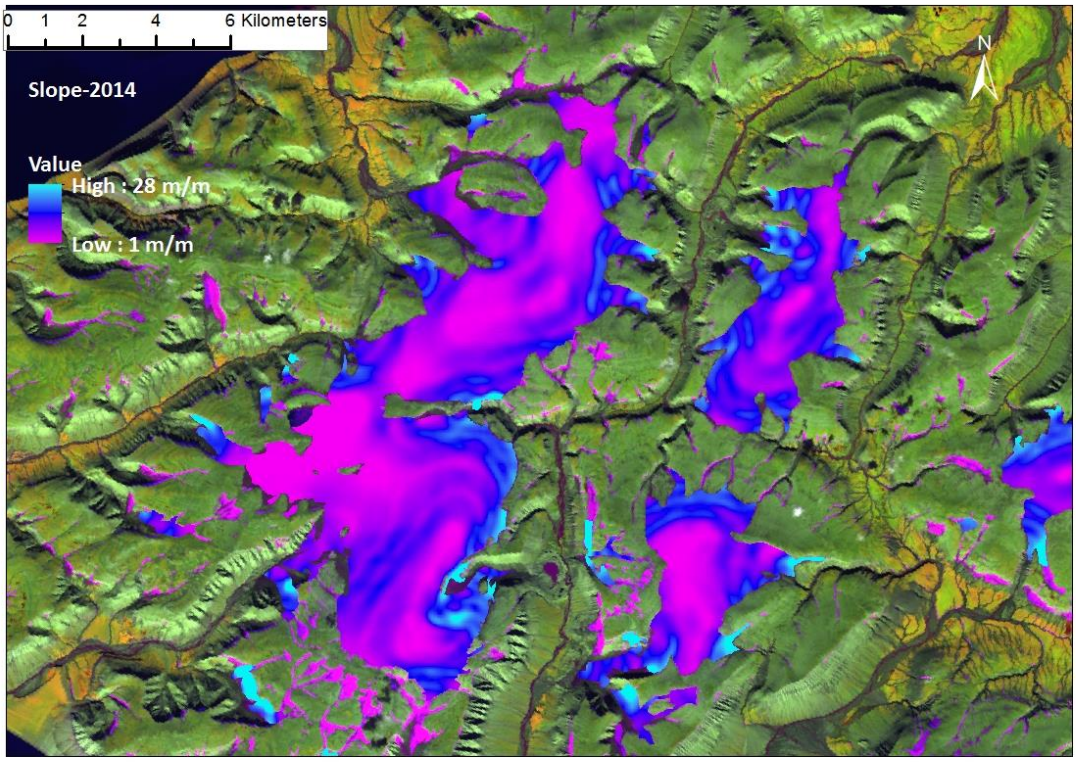

Figure 10; Slope map as for 2014 ice bodies. The slope derived from the DEM and surface area of the glaciers. The minimum slope is set at one, to prevent unlimited ice thickness. False color satellite image from landsat 8, band colors 4, 5, 1.

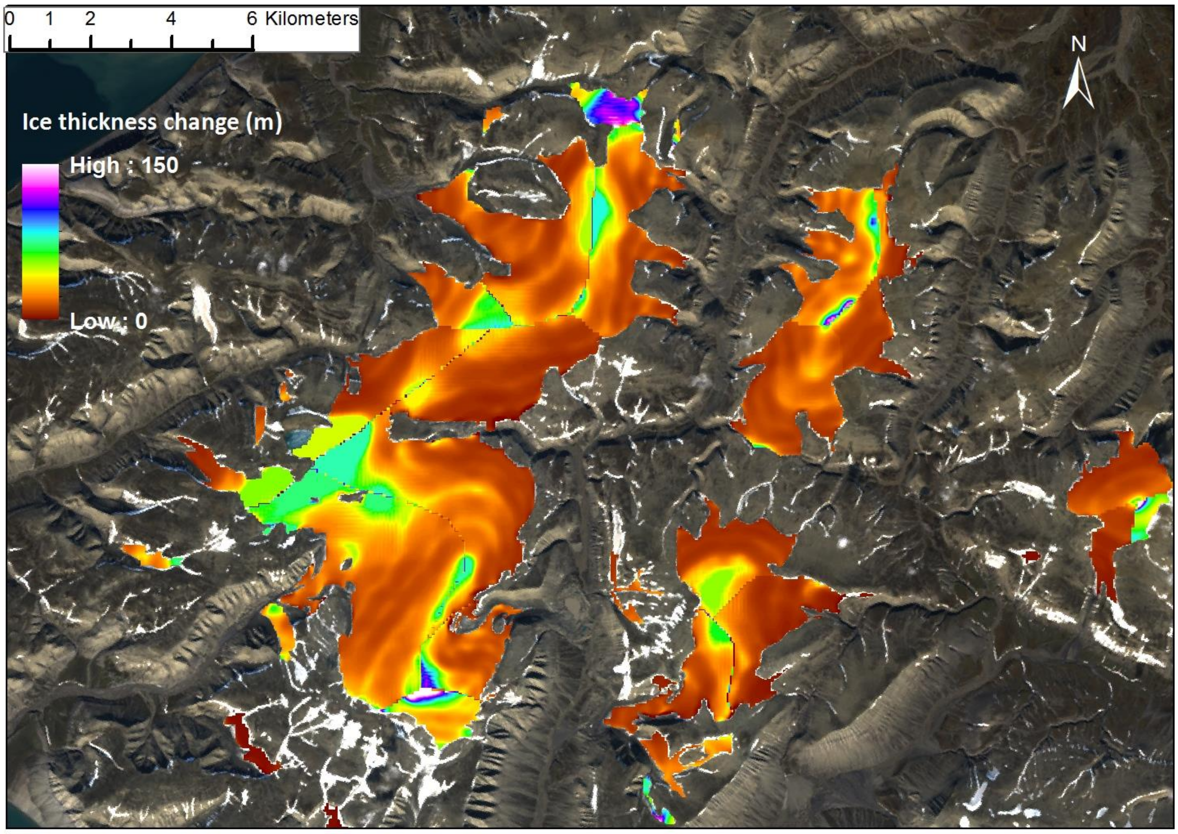

Figure 11; Ice thickness change from 1971 to 2014, calculated for different polygons in each ice body. Thickness is based on Weertman's sliding law: increase in thickness leads to ice flow.

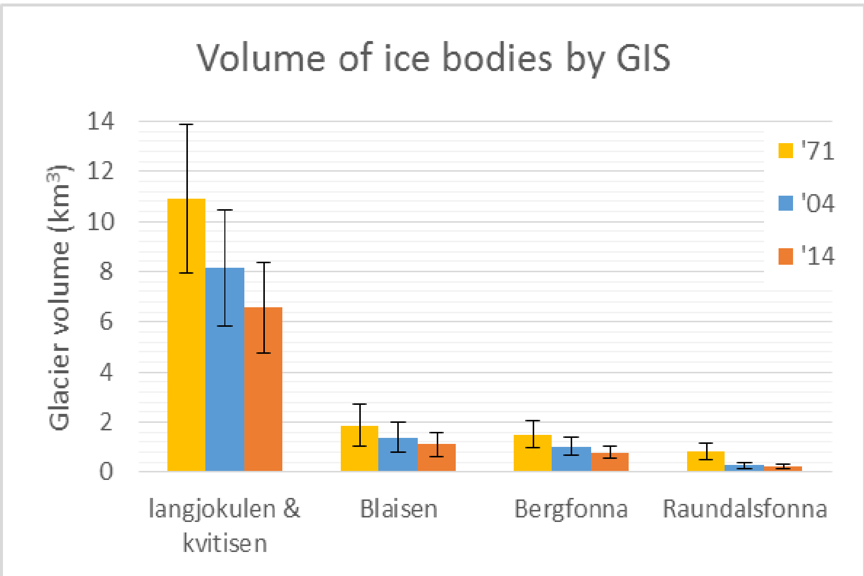

Figure 12; Volume of ice bodies as calculated with GIS based on Weertman's sliding law.

4.2 Modelling glaciers and meltwater

4.2.1 Calibration and initiation

The model is initialized by the ice thickness and extent as in 1971 based on the GIS-method. Then the model has been run with initial values based on literature for the parameters (table 5) and climate data as during the simulation time. The output is shown in maps for total ablation, accumulation, fluxes, ice thickness and the mass balance for the simulation period. The glacier extent is based on a minimum ice thickness of 1m water equivalent (w.e.). Calibrating the model has been done by trial and error: The ice thickness and area extent modelled after 43 years of simulation (figure 13) is compared to the ice thickness and area extent maps made by the GIS method, parameters have been calibrated to reach the best look-a-like result.

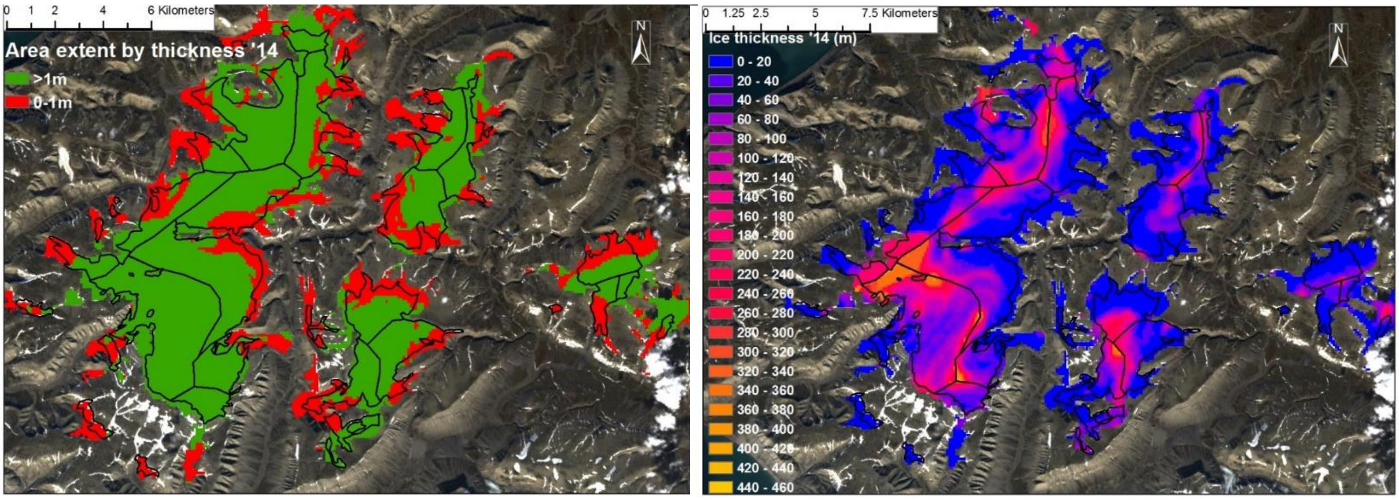

Figure 13; Ice extent and thickness as modelled after 43 years of simulation.

Table 5; Parameters used in the model, both for glacier thickness, extent and the hydrology modelling.

Parameter	description	Calibrated value	Unit
R	Material roughness	Unsign. influence ($2.3*10^9$ used)	N m^{-2} $s^{1/3}$
V	Bed rock roughness	0.1	-
TL	Temperature lapse rate	0.0058	°C m^{-1}
DDF	Degree day factor	14.5	mm °C d^{-1}
C	Aspect dependence of ddf	-0.03	-
ρ	Ice density	916.7	Kg m^{-3}
g	gravitational acceleration	9.81	m s^{-2}
maxS	Maximum soil moisture storage	0.0375	m
ETc	Correction factor for ET	0.086	Mm $°C^{-1}$
CN	Curve number	97	
Kc	Crop correctin factor for ET	0.2	
Rc	Recession constant for groundwater flow	$4.2*10^{-4}$	
Kx	Recession constant for flow	0.98	
Qi	Initial discharge	4.5	M^3/s
Sf	Fraction of snow ablation that results in runoff	0.95	
Gf	Fraction of ice ablation that results in runoff	0.8	

4.2.2 Data sets

Precipitation

The total precipitation at Edgeøya is the sum of rain and snowfall per cell. Whether precipitation falls as snow is determined by the temperature, assumed is t<0ºC is the baseline for snowfall, a temperature lapse rate is used. Precipitation in 43 years of simulation is a total of 8.3m, with an average of 0.19m per year. Most snow is fallen at higher latitudes and in the valleys as rain. There is no precipitation correction used for wind direction, this results that at every location the same amount of precipitation is fallen. Figure 14 shows the Rain and Snow map of NW Edgeøya.

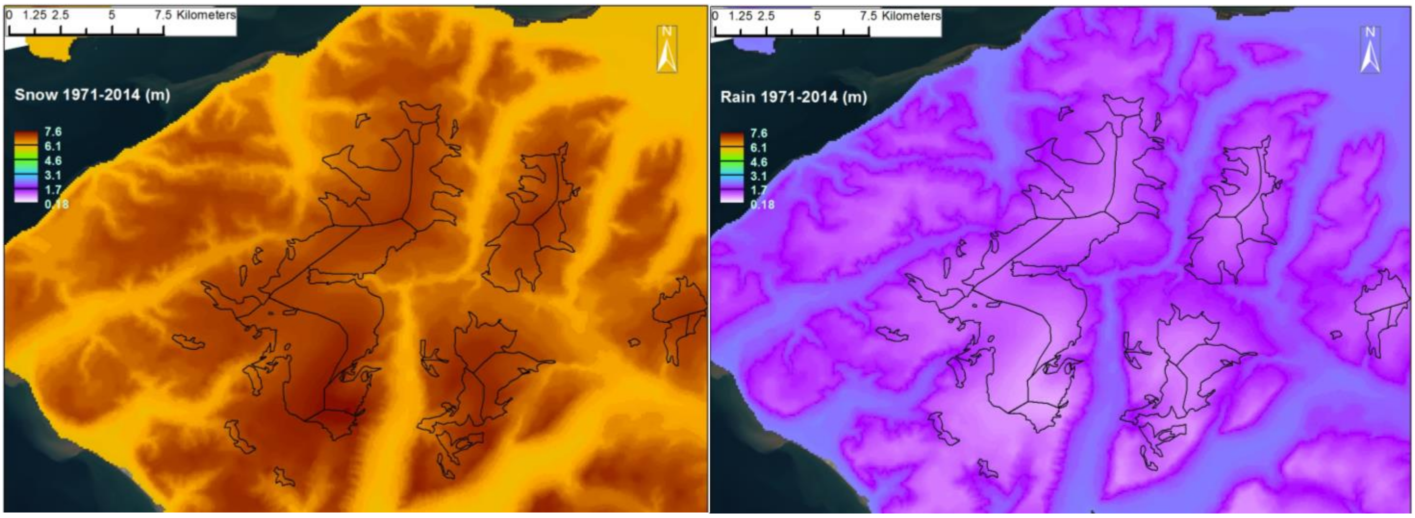

Figure 14; Rain and snow spatial distribution

4.2.3 Key processes

Mass balance

Combining the results of ablation, precipitation and the net flux of ice, the mass balance map has been produced (figure 15 a-c). The mass balance has a negative budget at the end of the simulation period, with an average loss of -40m during the simulation period (-0.93m/yr) resulting in rapid ice volume decrease. The first two years of the modelling show a mass balance at the highest altitude of +0.4 m (0.2m/yr) and an average of -1.7m (0.85m/yr), the last two years of the model has a positive mass balance at the highest altitude of 0.3m (0.15m/yr) and an average of -3.7m (-1.85m/yr) showing an increased mass loss with time.

Ablation

Ablation is mainly dependent on the slope and dependent on the Degree Day Factor. Temperatures have been increasing by 3.14 °C in the last 43 years as shown in figure 6 and the warming trend is increasing with time, as shown with the trend line. The main reason is an increase in winter temperatures, since summer temperatures are not significant warmer. The degree day factor dependent on the aspect is show in figure 16 when DDF is 14. Combining the two results gives an average ablation of ca. 60m during the simulation period (-1.40m/yr), with higher ablation in lower elevation areas. The low ablation rates at glacier snouts is due to the limited glacier ice thickness at those locations (figure 16).

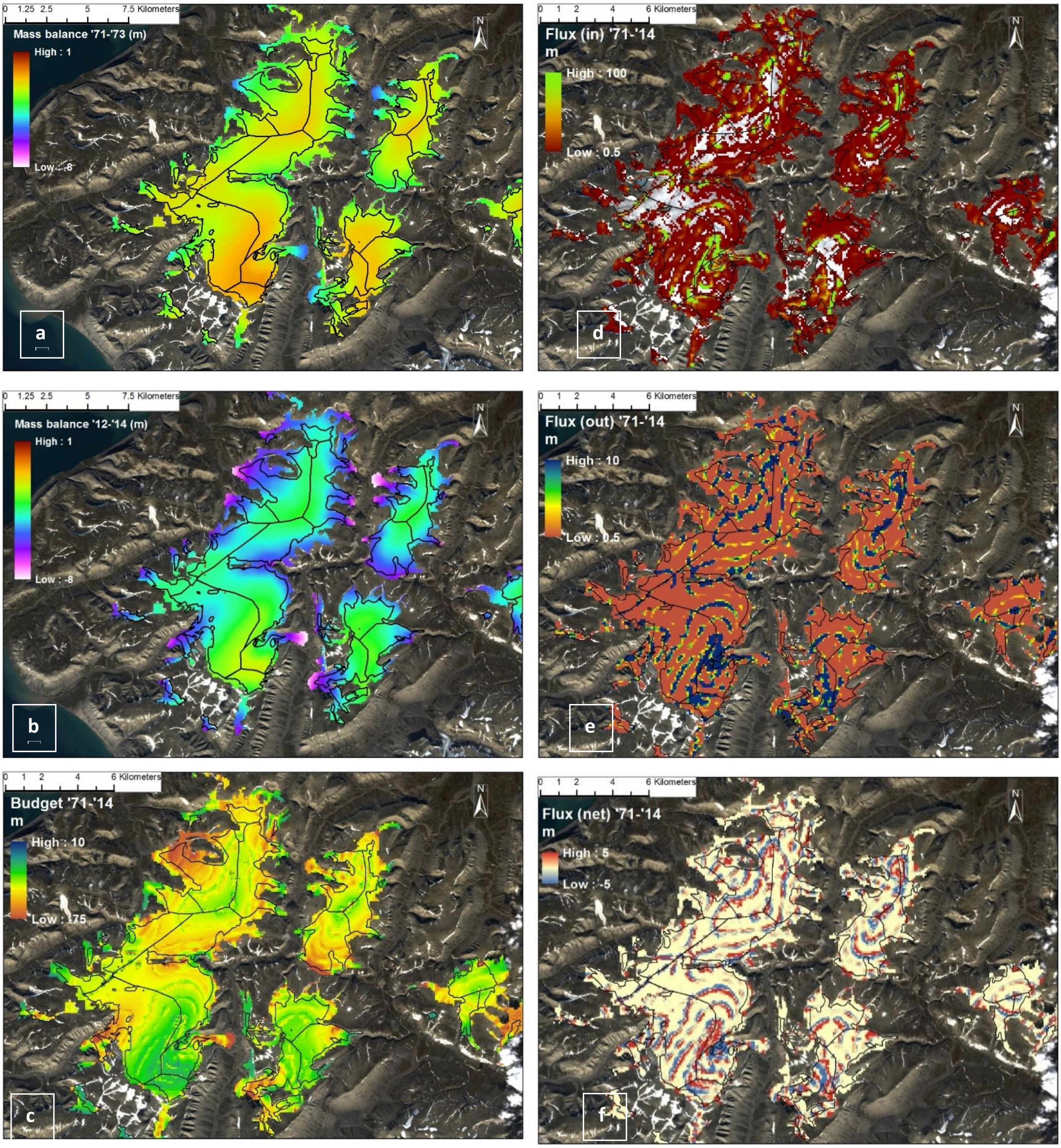

Figure 15; Mass balance and ice fluxes at the northernmost ice cap of Edgeøya. Mass balance for the years 1971 to 1973 (a) and 2012 to 2014 (b) are the sum of the modelled budget of the first and last two years of the model and the total budget after 43 years (c). The in- (d) and outgoing (e) ice flux for every grid cell, and the net ice flux (f) show the slow movement of ice in these ice caps.

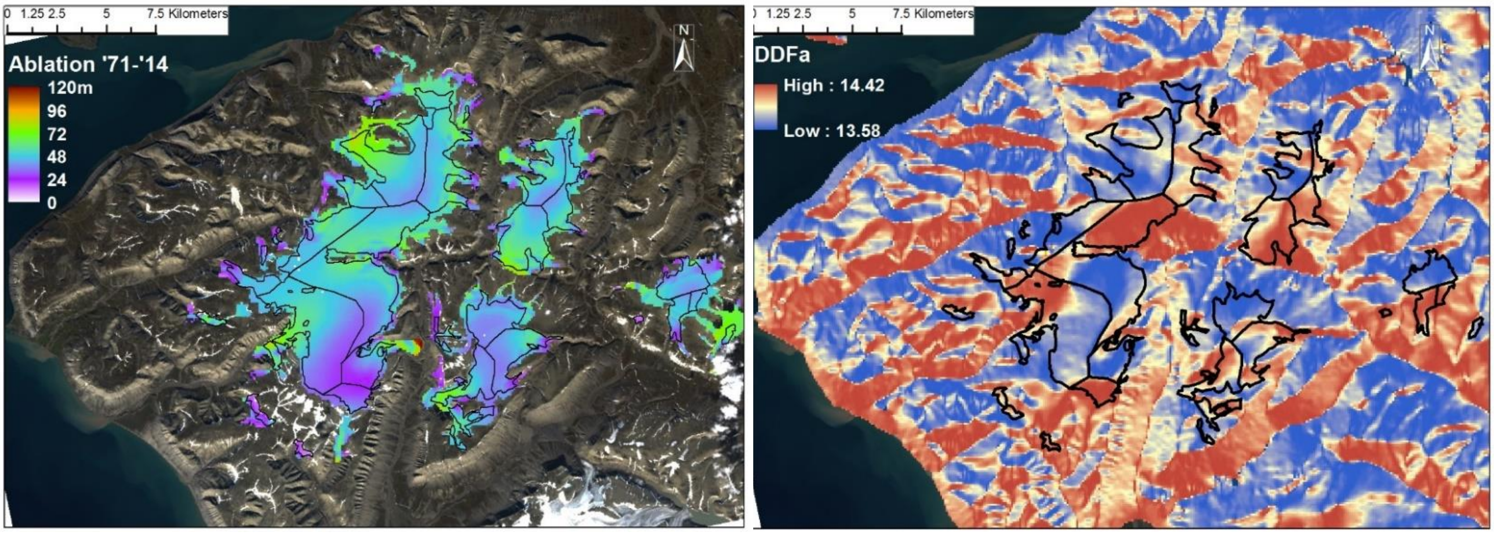

Figure 16; DDF spatial distribution based on the aspect (left) and the total ablation after the model simulation from 1971-2014 (right).

Fluxes

The flux of ice in and out of each cell is made visible in figure 15 d-f, and represents extremely low values compared to average glacier flow. Highest values are recorded in higher elevation areas (accumulation zone) and in bands on specific heights. The latter is due to an error in the smoothness of the used DEM, since it is based on the contour lines of a topographic map. In the accumulation zone, flux(in) has values up to 100m and flux (out) up to 10m during the simulation period. The main ice cap has low values of maximum 0.5m of ice flow per cell during the simulation period (0.01m/yr). A reason for this could be the shear stress being lower than the equilibrium shear stress, since ice thickness is beneath the equilibrium ice thickness under ideal conditions (and not a warming world).

Hydrology

The model has been run with variables as stated in table 5, and due to lack of field data of river discharge, the model is not calibrated. Therefore numbers presented here should be interpreted with precaution and seen as relative numbers that can be compared with each other and compared in time. To allow the model to stabilize from initial input values, all data is shown here from day 154 (1st of January 1972).

The drainage area together with its glacierized part is visualized in figure 17 and summarized in table 6. Obviously, the larger the drainage area the higher the total runoff (Qtot), and the larger the glacierized area, the larger the glacier part of the total runoff (Qglacier). Percentage glacier loss from 1971-2014 per drainage area varies widely from 18.1 to 48.5% (1 to 15.7 km^2), but also the part that is glacierized varies (0 to 30.4%). This challenges the interpretation of potential runoff increase or decline, since a large increase in mass loss could result in an increase in runoff (more ice melt) and a decrease in runoff (decreased glacierized area).

Figures of discharge per drainage area, for total discharge and the contribution of glacial melt together with analysis of seasonal fluctuations follow below.

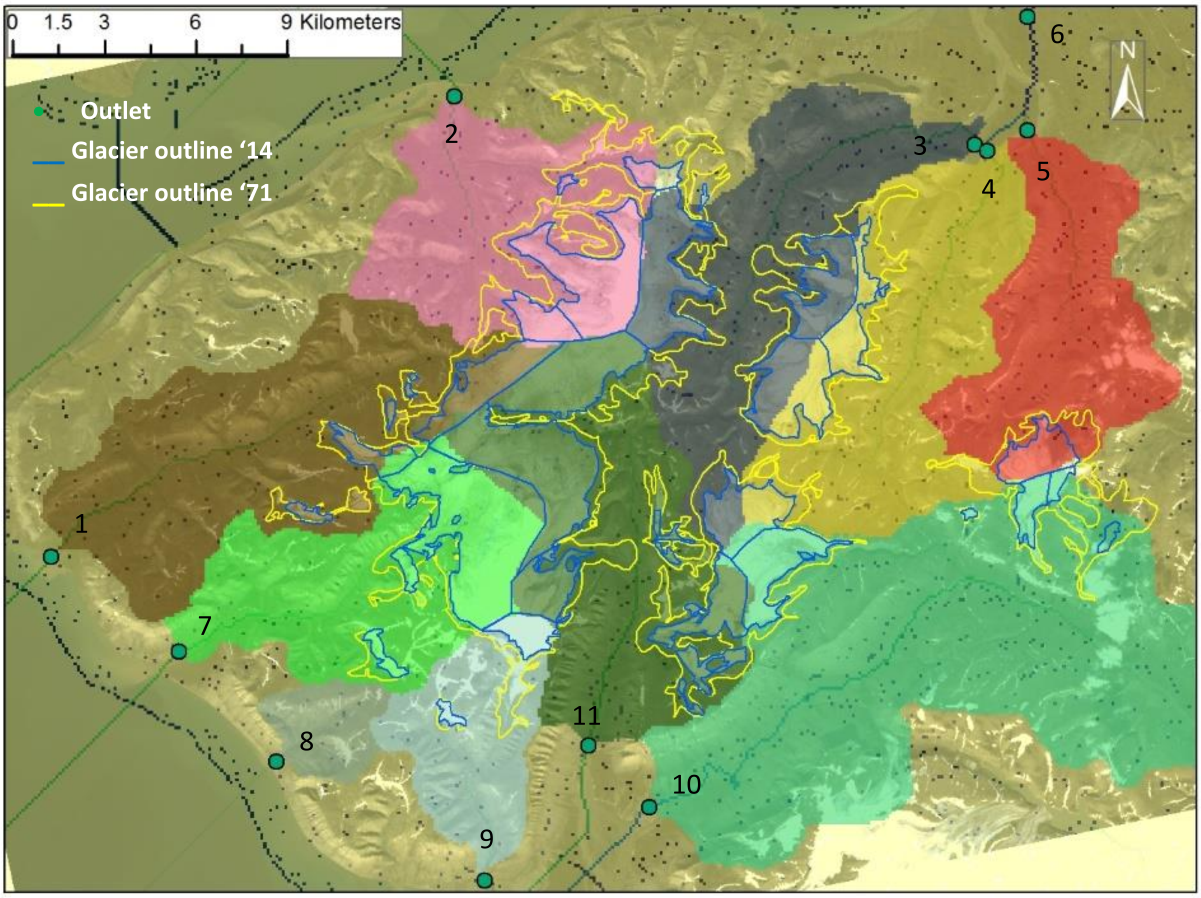

Figure 17; Map with all drainage areas as used in the model. Green dots are the outlet points in which the discharge is calculated and visualized. Numbers are the same as in table 6.

*Table 6; Drainage area and the decline of glacier area in percentage and km^2. The Qglacier and Qtot is defined as the total km^3 glacier meltwater and river discharge, respectively, after 43 years of model simulation. *area number 6 is the sum of areas 3, 4 and 5.*

Drainage area	Drainage area (km^2)	Glacier area in 1971 (%)	Glacier area in 2014 (%)	Glacier loss 43 yr (km^2)	Glacier loss 43 yr (%)	Qglacier /Qtot 43 yr (%)	Qtot 43 yr (km3)	Qtot (mm/yr)	Qglacier (mm/yr)
1	79.8	14.6	8.3	5.1	43.5	42.8	0.83	244	105
2	58.4	32.9	19.6	7.8	40.5	68.8	1.19	349	241
3	74.4	34.4	22.4	8.9	34.8	67.5	1.45	426	288
4	68.4	23.6	12.1	7.8	48.5	57.9	1.00	293	170
5	50.0	7.9	5.9	1.0	26.1	33.1	0.44	129	42.7
6*	209	21.8	13.4	17.7	38.9	57.2	2.98	874	501
7	57.2	36.0	29.5	3.7	18.1	68.0	1.05	308	210
8	10.3	0.0	0.0	0.0	0.0	0.0	0.06	17.6	0.00
9	28.9	14.5	7.6	2.0	47.6	40.2	0.28	82.3	33.26
10	139	10.2	5.7	6.4	44.7	34.8	1.25	367	129
11	77.2	50.8	30.4	15.7	40.1	74.6	1.90	558	418

The total discharge is plotted in figure 18 and shows a clear distinguishing seasonal trend with high summer (peak flow) and low winter runoff (base flow). Since glacier melt is forced in the model by temperature and ablation, in winter the glacier melt is zero (figure 19). The remaining runoff in Qtotal in winter is by groundwater flow and rain at lower (warmer) areas. In summer, peak discharges of 150 m^3/s are reached as the sum of all outlet points. These discharges do not all enter the rivers directly but have a delay and some is stored in soils and recharged to groundwater, therefore, the total discharge of all outlet points show peak values of 35 m^3/s maximum. On average, the annual average glacier flow in total is in the range of 1.2 and 7.5 m^3/s (fig. 20). The colors in figure 20 show the different drainage areas and reveal that larger runoff values correspond with larger glacierized and drainage area.

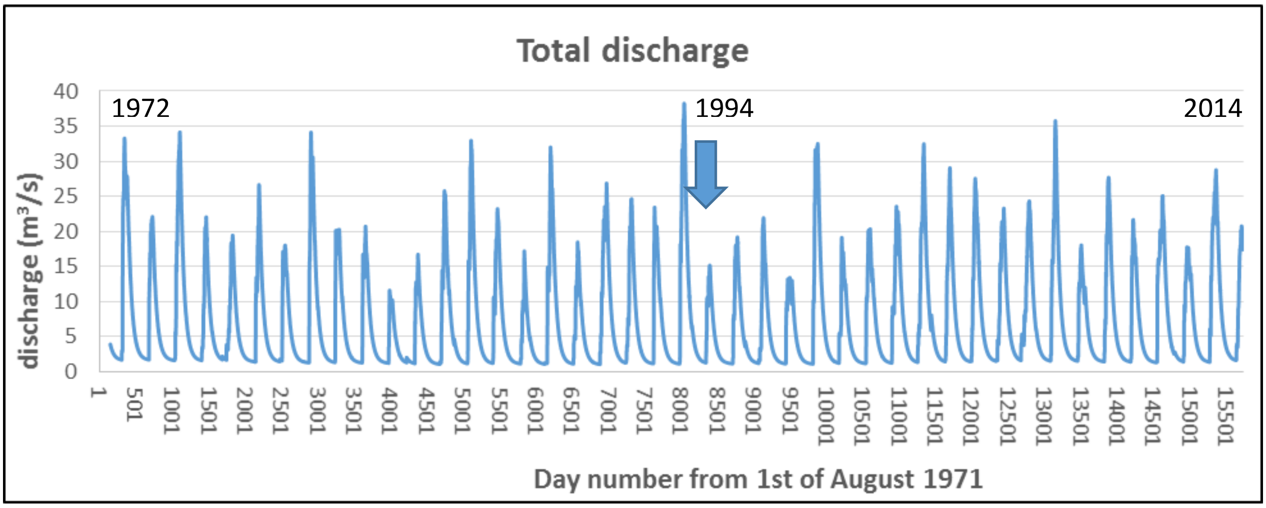

Figure 18; Total discharge as the sum of discharge at all outlet points. Total discharge is the sum of groundwater and surface water measured at the outlet point.

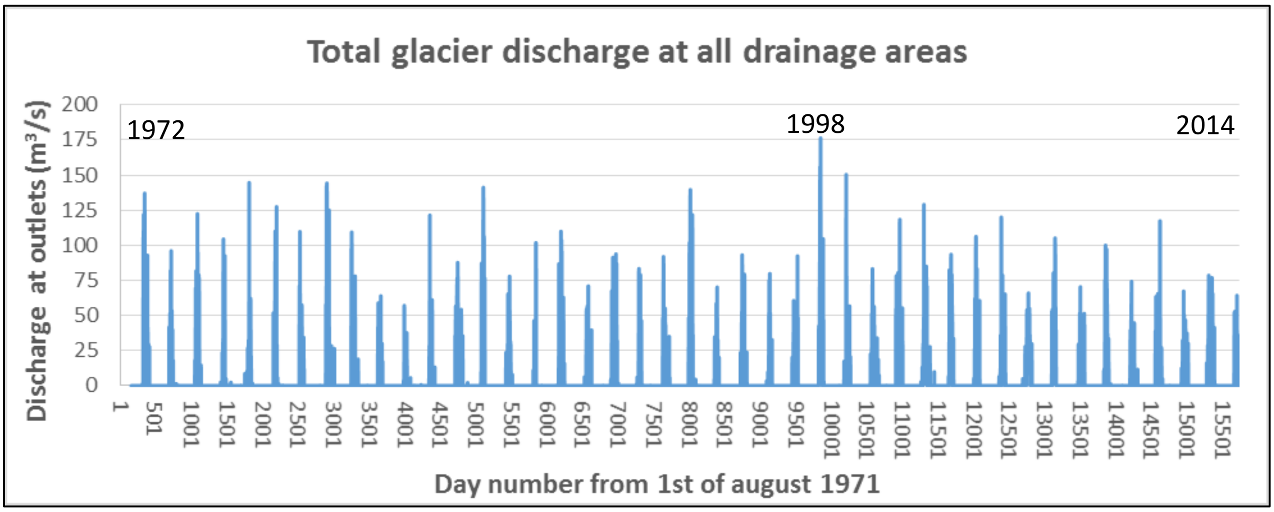

Figure 19; Total discharge from glacier melt only as the sum of discharges from all outlet points.

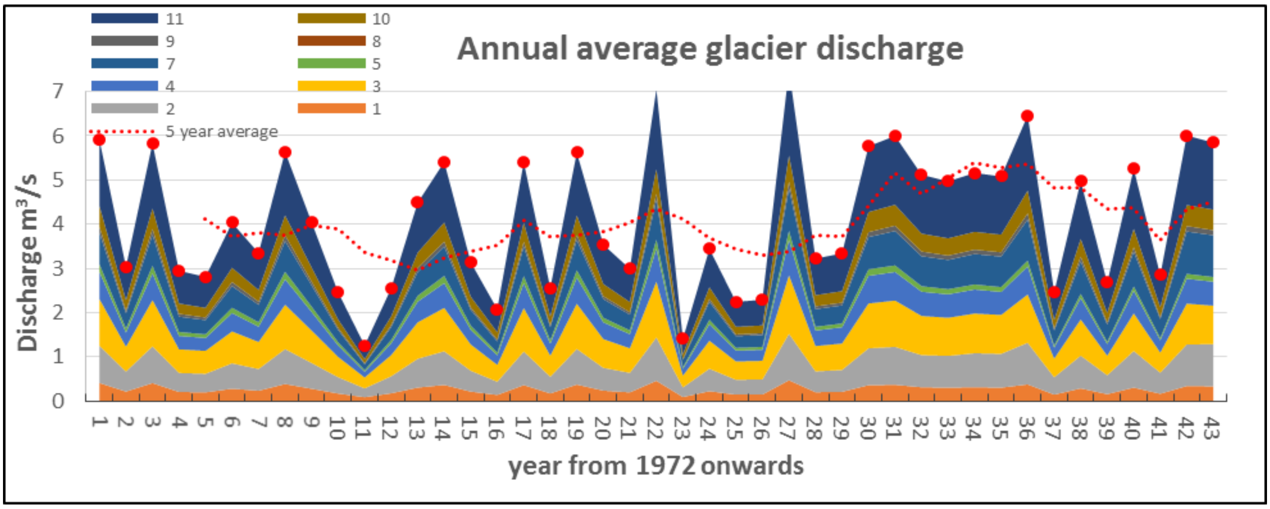

Figure 20; Annual average glacial discharge as cumulative of the different drainage areas. Numbers correspond with drainage area numbers as in figure 18.

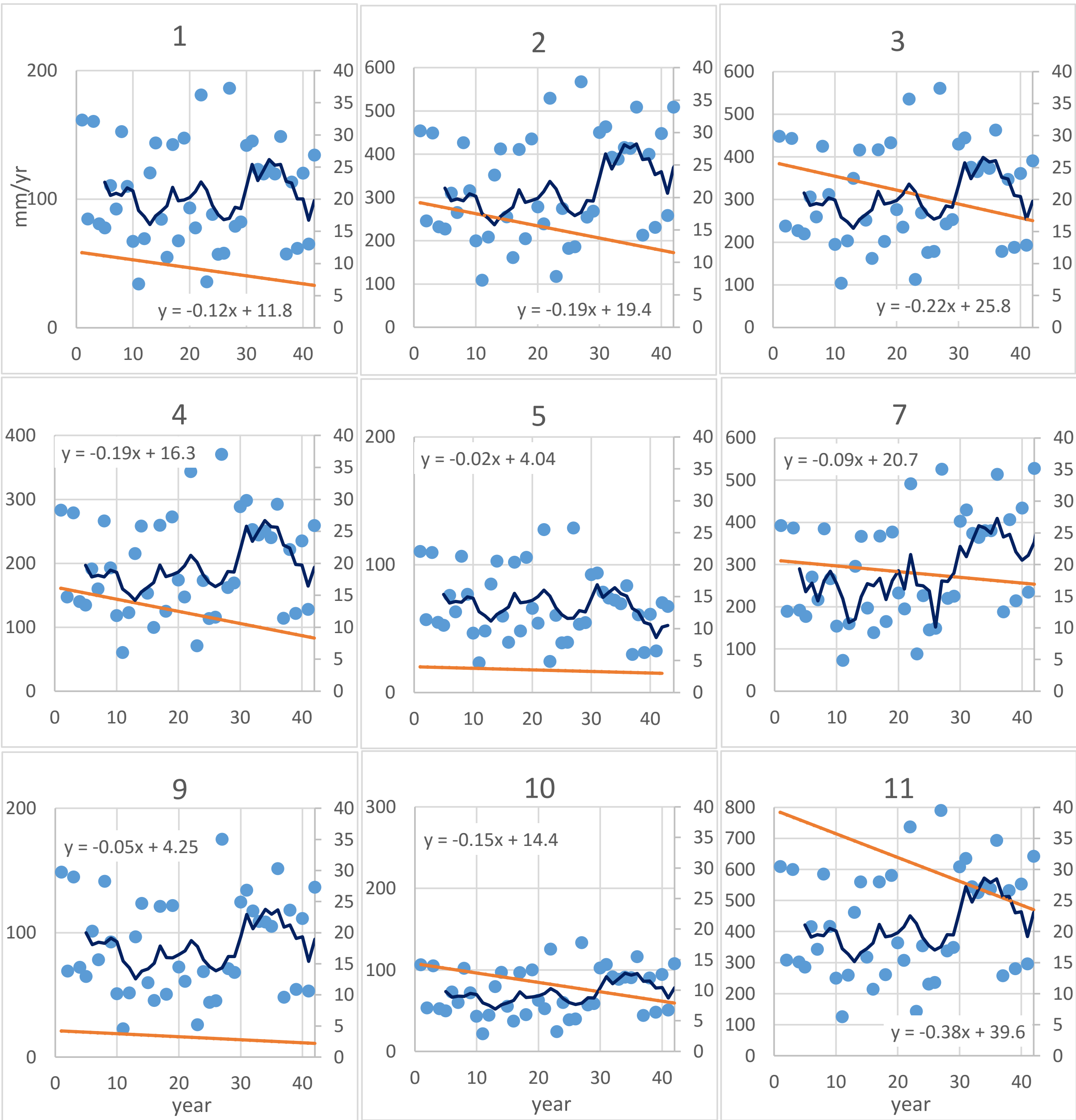

Figure 21; Qglacier Mm/yr for every drainage are, calculated from the average discharge per year and corrected for area.

In figure 21, the glacier meltwater discharge is noted in mm/yr and therefor corrected for the drainage area. The five year average trend line shows that the whole area is sensitive to the same changes, not well corresponding with precipitation (figure 4) or annual average temperature (figure 6). Drainage area 2 and 11 have an increasing glacial discharge and a fast ice volume decline rate, drainage areas 3, 4 and 10 have a fast ice volume decline rate as well, but do not increase in discharge as large. The only drainage area that is decreasing glacial discharge is research area 5, the ice volume is very low compared to other area's and the absolute losses are low as well ($1.0km^3$).

The glacial meltwater discharge as percentage of the total discharge is visualized in figure 22. First, the percentage of glacial water in the total discharge varies largely per drainage area from around 30% (areas 5 and 10) to 70% (areas 2, 3, 7 and 11). This is highly dependent on the glacierized area (table 6), with increasing glacial meltwater contribution with increasing glacierized area. Only drainage area 7 shows a decline in glacier meltwater contribution, and this is the area with the lowest glacier loss from 1971 to 2014 in percentage (18.1%). If this correlation is significant needs further investigation, since the second-lowest glacier area loss in percentage is area 5, which shows a slight decrease in percentage glacier area (26.1%). The drainage area of area 5 and 7 are of similar size, but the percentage ice covered does vary (7.9% area 5, 36% area 7). Another aspect is ice thickness, the ice is thin (<40m) in drainage area 5 and thick in area 7 (up to 400m), making area 5 more sensitive to changes.

The rain contribution to the river discharge is 193mm/yr on average for every drainage area since no precipitation distribution corrected in implemented in the model. The groundwater part of the total discharge is left out here since it is highly dependent on the storage factor. The storage factor is complicated in permafrost areas which have increasing active layer depth with increasing temperatures. The role is plays in this area is not well investigated yet, and no field data is available for calibration.

To elucidate any increase in discharge, as stated in the research question, we need to take a closer look at the graphs. Figure 19 shows no increase in peak flow with time, instead the peak shows a slight decrease for the last 16 years. Figure 20 shows a slight increase in total discharge for the last 26 years and figure 18 elucidate that the baseflow is increasing since then as well. Besides increasing run off, since the 1990's the amount of days with runoff does increase also (figure 23), and this is mainly due to an increase in the amount of days with glacier discharge above 5 m^3/s (figure 24). Figure 24 and 18 together show that there is an increase in days with moderate and base flow and not in peak flow.

In September the average day temperature is around zero. With increasing air temperature, this month is expected to elucidate the largest changes with glacial melt. Instead, figure 26 and 27 show that the amount of runoff in summer (June-august) is not increasing, and that the summer melt season is not lengthened into September for this research area.

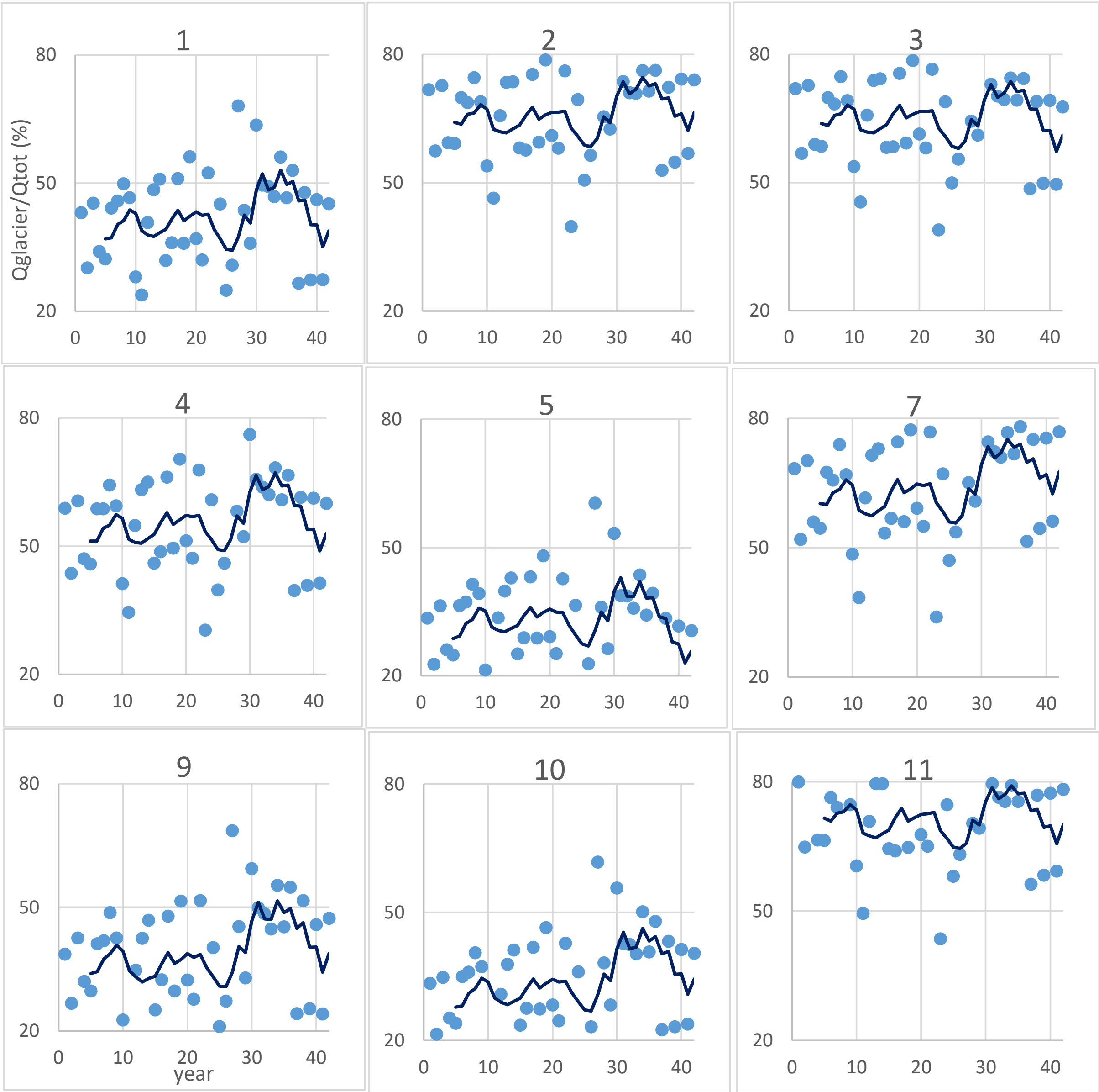

Figure 22; Percentage of Qglacial in Qtotaal, corrected for each drainage area.

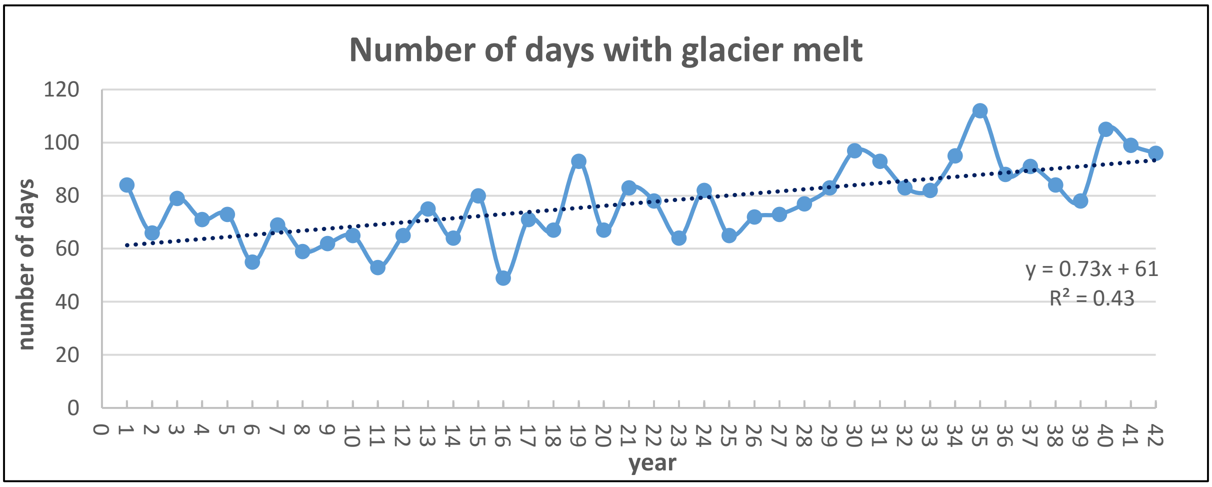

Figure 23; Days with ice melt (1) and no ice melt (0) with a minimum daily discharge above 5m³/s when there is ice melt. An increase in the number of days with ice melt is visible from year 23, corresponding with 1995.

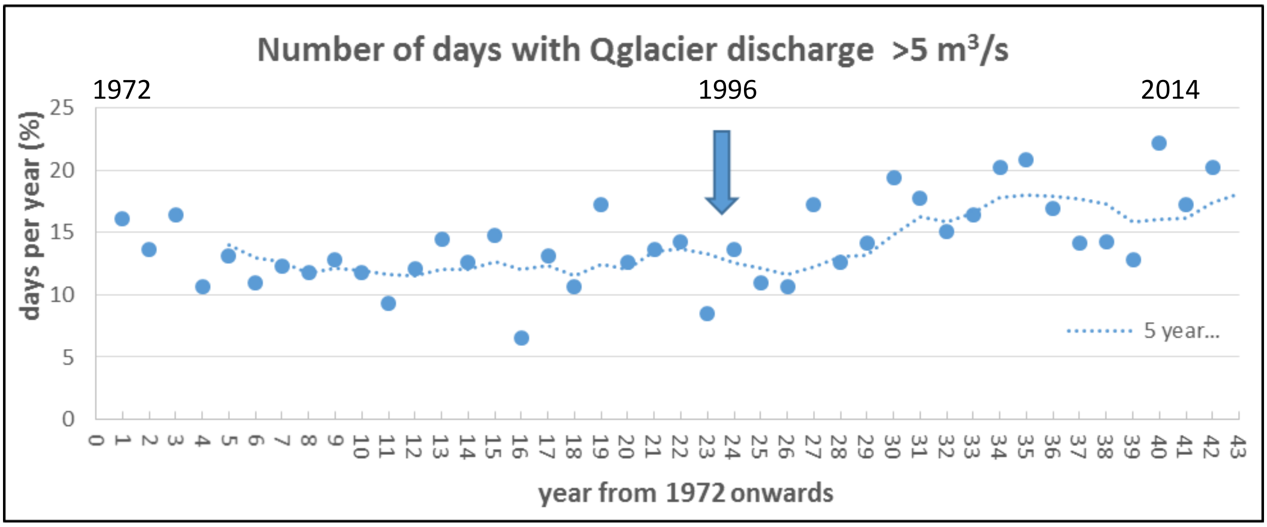

Figure 24; Number of days with discharge above a minimum of 5m³/s, to show if there is increase in days with moderate flow. Trendline is the 5-year average

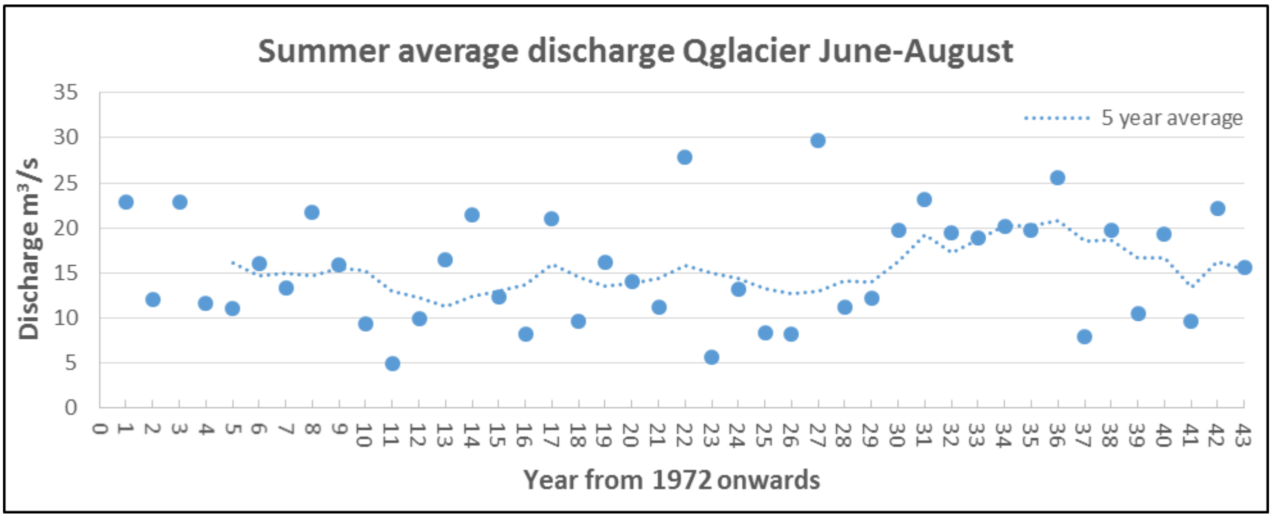

Figure 25; Summer discharge for the months June, July and August with the 5 year average trendlne.

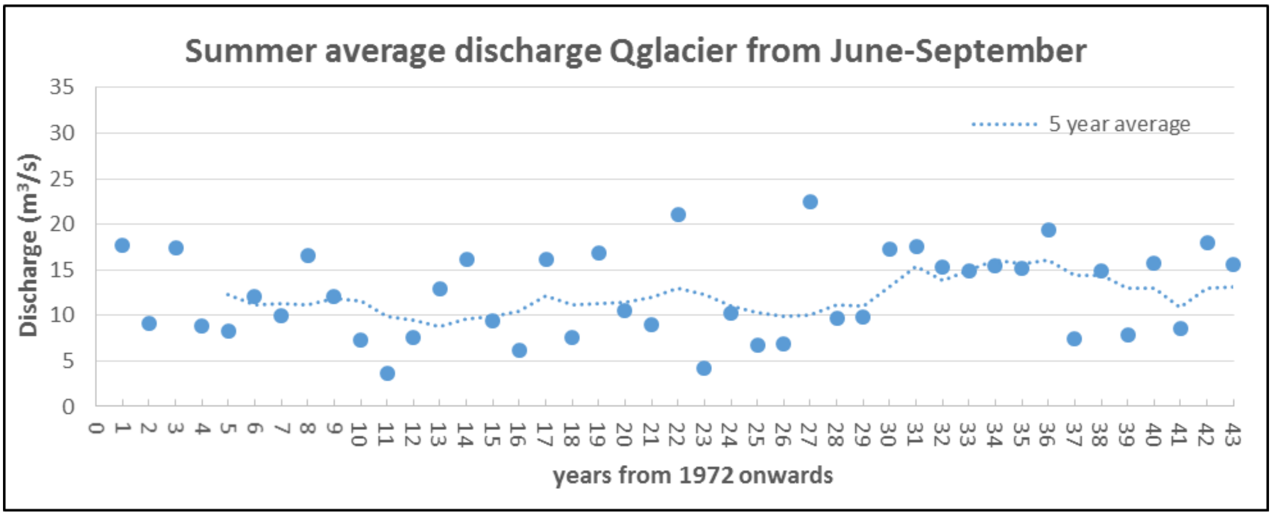

Figure 26; Summer discharge for the months June, July, August and September with the 5 year average trendline.

4.3 Carbon degradability and flux

4.3.1 Water isotopes

The water isotopic composition is plotted in an $\delta^{18}O/\delta D$ diagram and shows a strong linear correlation (figure 27). The GMWL, which is the global correlation between $\delta^{18}O$ and δD ($\delta D = 8*\delta^{18}O + 10$) (Craig, 1961) is plotted together with the LMWL (Yde et al., 2012); IAEA/WMO, 2006) which is based on measurements at Isfjord radio, Svalbard. The data fits the LMWL both for precipitation, glacier ice and river samples. To determine if phase transitions as melt and evaporation have altered the isotopic signal, the offset between the sample data and LMWL, the δD-excess ($d = \delta^{18}O - 8\delta D$), is plotted against δD (figure 28). This shows the slight heavy offset from the LMWL for most water samples.

The water isotopic signatures of the ice samples are -14.6±0.41‰ and 97.9±3.4‰ and for the precipitation samples -6.0±0.69‰ and -44.6±4.1‰ for $\delta^{18}O$ and δD respectively. All river samples fit between the ice and precipitation data points with an average of δD -86.2±7.1‰ and $\delta^{18}O$ -12.8±0.83‰. The ice and precipitation data points are used as end member values to calculate the contribution of water that is derived from either of these sources. For %-glacier-derived water it is done for δD as:

$$\%\text{ glacier derived water } = \frac{\delta Driver - \delta Dprecipition}{\delta Dice - \delta Dprecipiation} * 100 \qquad (20)$$

Rivers receive on average 78±13% of their water from glacier sources. In proximity to the ice caps (<5km) measured δD values range between -70.5 and -102‰, but the δD gets more constant with longer distance from the ice cap to an average value of -91.4±2.9‰, as shown in figure 29.

Table 7; An overview of the organic matter sampling data with location and distance from ice and coast respectively

	Glacier from which the sample comes from	**Latitude**	**Longitude**	**Distance glacier**	**Distance coast**
River	Larsbreen	78.1985	15.5802	1.5km	3.6km
River	Longyearbreen	78.1981	15.5643	1.2km	3.8km
River	Staupbreen	77.0852	17.2971	<0.1km	<0.1km
River	Rosenbergdalen-0	78.0692	20.8808	15.2km	<0.1lkm
River	Rosenbergdalen-1	78.0753	20.9056	14.2km	1km
River	Rosenbergdalen-2	78.0813	20.9361	13.2 km (valley)	2km
River	Rosenbergdalen-3	78.0894	21.0221	11km (valley)	4.2km
River	North-Agardhbukta	78.1425	18.9742	<0.1km	5.0km
River	Plurdalen	77.6466	21.2759	19km (valley)	2.7km
River	Kvalpuntfonna	77.6440	21.2854	8.0km	2.8km
River	Kvitkapa	77.3875	22.6747	3.6km	<0.1km
Snow	Rosenbergdalen-snow	78.0797	20.9105	<0.10km	0.8km
Tributary	Rosenbergdalen-side 1	78.0828	20.9330	1km to plateau	2.2km
Tributary	Rosenbergdalen- side 2	78.0778	20.8684	1km to plateau	2.5km
Tributary	North-Agardhbukta-side	78.1287	18.8582	1.8km	4km
River	Freemanbreen-east	78.2668	21.8679	1.4km	<0.1m
River	Freemanbreen-west	78.2594	21.6794	1.8km	<0.1km
River	Ulvebreen	78.1853	18.9742	<0.1km	0.5km
Ice	Ulvebreen (ice)	78.2000	18.6833	0km	2.2km
Ice	Freemanbreen (ice)	78.2693	21.7908	0km	0m

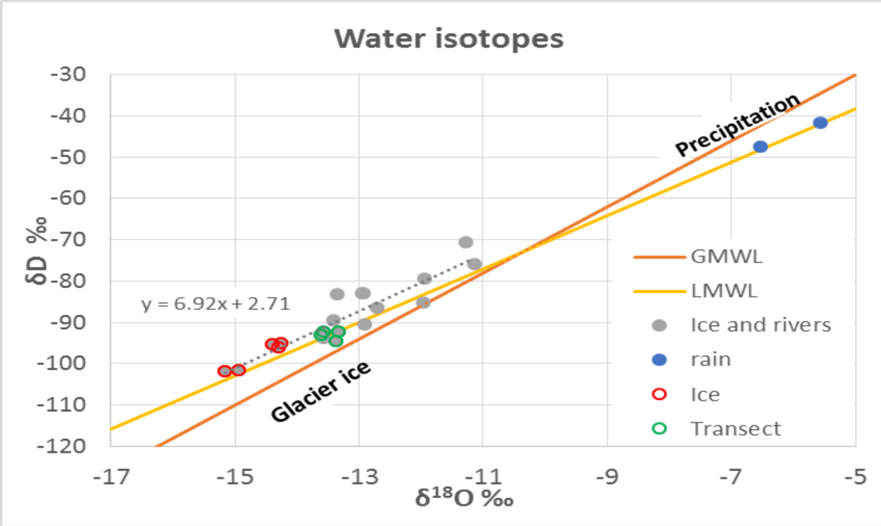

Figure 27; Plot of the water isotopic composition of the water samples. The data is compared to the GMWL (orange) and LMWL (yellow). The precipitation (blue) and glacier ice samples (red circle) are defined as endmembers, since all other samples have intermediate values. The transect samples from Rosenbergdalen (green) are distinguished from the ice and river samples (grey).

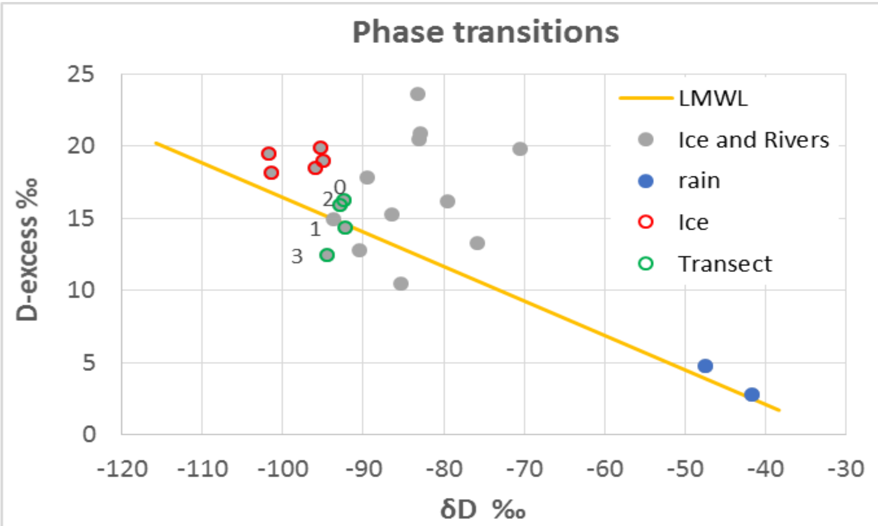

Figure 28; Deuterium-excess of the water samples compared to the LMWL (yellow). Off-LMWL samples have undergone phase transition(s). Colors are similar as in figure 27.

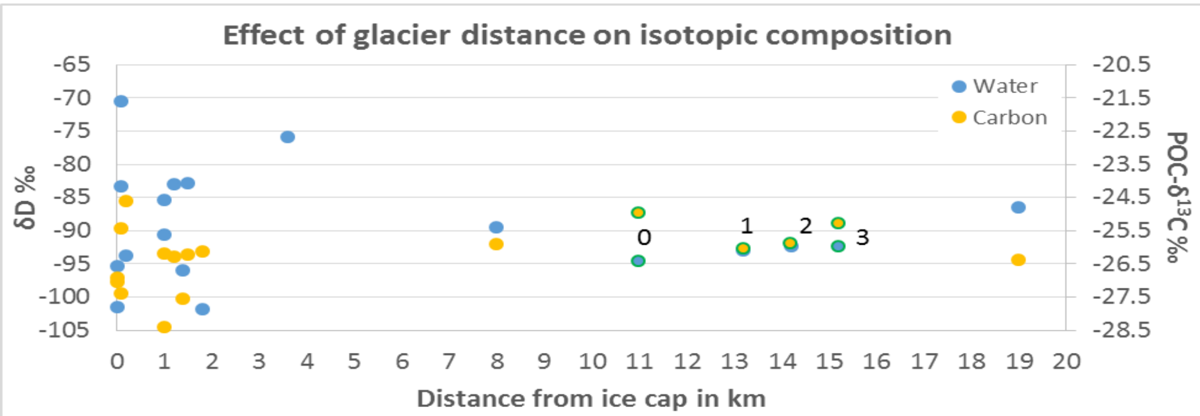

Figure 29; water and POC-isotopic composition of river samples with distance from the main ice cap (glacier). Numbers indicate samples from the Rosenbergdalen transect (also green circled) with 0 closest to sea and 3 closest to ice cap.

4.3.2 TSS, Organic Carbon and bioavailability

POC samples vary widely with values between 0.05 and 83 mg/L with higher values when TSS is higher as found in figure 30 and figure 32. The TSS can be considered as a proxy of flow velocity, with higher velocities carrying more suspended matter in the water column. Higher POC values are therefore found in streams with high discharges, but are also found in streams with very low flow velocities and more organic material (life) in the water column. On average 1.2% of the TSS was POC. The DOC varies between 0.05 and 0.55mg/L. There is no correlation between the amount of POC and TSS with DOC values (figure 30) in river and ice samples.

The $\delta^{13}C$-isotopic composition of POC is -26.8±0.72‰ for ice, -25.9±0.68‰ for rivers, and 27.3±1.6‰ for tributaries. As the error margins are overlapping the isotopic difference between river samples and ice samples is not significant. However, there might be a non-linear with water source in which the $\delta^{13}C$-POC is heavier in samples with a higher contribution of glacier-derived water and heavier when glacier-derived water contribution is low (figure 31). The glacier samples are highly variable in $\delta^{13}C$-POC and are an endmember for the river $\delta^{13}C$-POC values. Similar as with the water isotopic composition, the carbon isotopes seem to level out (-25.7±0.52‰) when the distance from the ice cap increases (>5000m) (figure 29). Last, figure 32 shows that there is no significant correlation with POC and TSS amount for the ice samples.

Bioavailability measurements show variable results, not all show DOC loss and for some samples the amount of DOC increased throughout the experiment for unknown reasons. The typical degradation rate is 14±8.5% with a maximum of 27% loss in 14 days.

*Table 8; Water source information ($\delta^{18}O$ and δD) together with TSS and organic matter data (^{13}C-POC, POC and DOC). * End member present day rain; ** end member glacier ice $^{+}$ is derived from 250ml frozen, unacidified samples.*

	Source				Organic carbon			
Glacier from which the sample comes from	$\delta^{18}O$ ‰	δD ‰	Glacier water %	TSS mg/L	POC mg/L	POC %	$\delta^{13}C$ ‰	DOC mg/L
Larsbreen	-12.96	-82.8	72	$5.1*10^3$	40.4	0.80	-26.2	0.23
Longyearbreen	-12.93	-83.0	72	$2.6*10^3$	33.7	1.10	-26.3	0.18
Staupbreen	-11.29	-70.5	49	$1.3*10^3$	13.0	0.95	-25.4	0.15
Rosenbergdalen-0	-13.58	-92.4	90	$1.5*10^2$	2.33	1.74	-25.3	0.21
Rosenbergdalen-1	-13.33	-92.3	90	$4.5*10^1$	0.20	1.41	-25.9	0.11^{+}
Rosenbergdalen-2	-13.62	-93.0	91	$8.3*10^1$	0.41	1.53	-26.0	0.26^{+}
Rosenbergdalen-3	-13.38	-94.6	94	$2.3*10^2$	2.71	1.41	-25.0	0.44
North-Agardhbukta	-13.36	-83.3	73	$3.7*10^2$	7.86	2.06	-27.4	0.12
Plurdalen	-12.72	-86.5	79	$5.4*10^2$	2.91	1.22	-26.4	0.16
Kvalpuntfonna	-13.42	-89.5	84	$2.8*10^2$	2.32	1.34	-25.9	0.12
Kvitkapa	-11.15	-75.9	59	<0.1	<0.1	X	X	0.15
Rosenbergdalen-snow	-13.58	-93.7	92	$2.9*10^3$	75.5	1.90	-24.6	x
Rosenbergdalen-side 1	-11.97	-85.3	76	$1.4*10^3$	0.42	5.84	-28.7	x
Rosenbergdalen- side 2	-12.92	-90.5	86	$3.1*10^2$	2.47	1.28	-26.2	0.53
North-Agardhbukta-side	-11.95	-79.4	65	X	X	X	X	X
Freemanbreen-east**	-14.31	-95.9	100	$3.4*10^3$	54.5	1.68	-27.6	0.24
Freemanbreen-west**	-15.16	-101.8	100	$1.2*10^3$	15.1	1.12	-26.1	0.17
Ulvebreen**	-14.39	-95.3	100	$2.1*10^2$	2.60	1.32	-27.0	0.05
Ulvebreen (ice)**	-14.95	-101.5	100	$1.2*10^2$	3.58	3.12	-26.9	0.52
Freemanbreen (ice)**	-14.26	-95.1	100	X	X	X	X	0.55
Rain 1*	-6.54	-47.5	0*					
Rain 2*	-5.56	-41.7	0*					

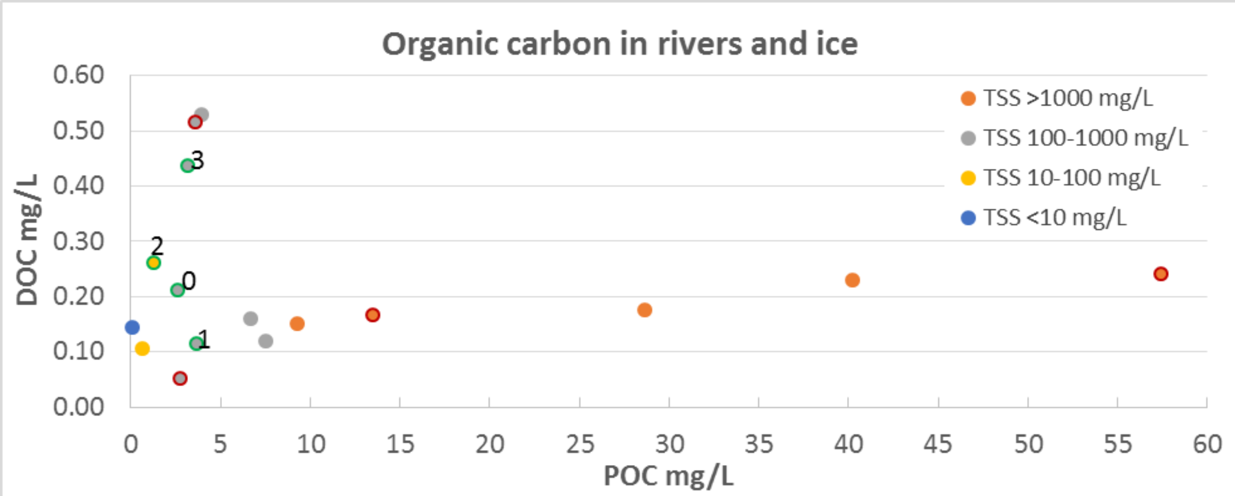

Figure 30; DOC and POC plotted with TSS as measured in the water and ice (red circles) samples. TSS is divided into four categories (<10 in blue, 10-100 in yellow, 100-1000 in grey, >1000 mg/L in orange). The transect samples are circled with green and numbers are as in Figure 29.

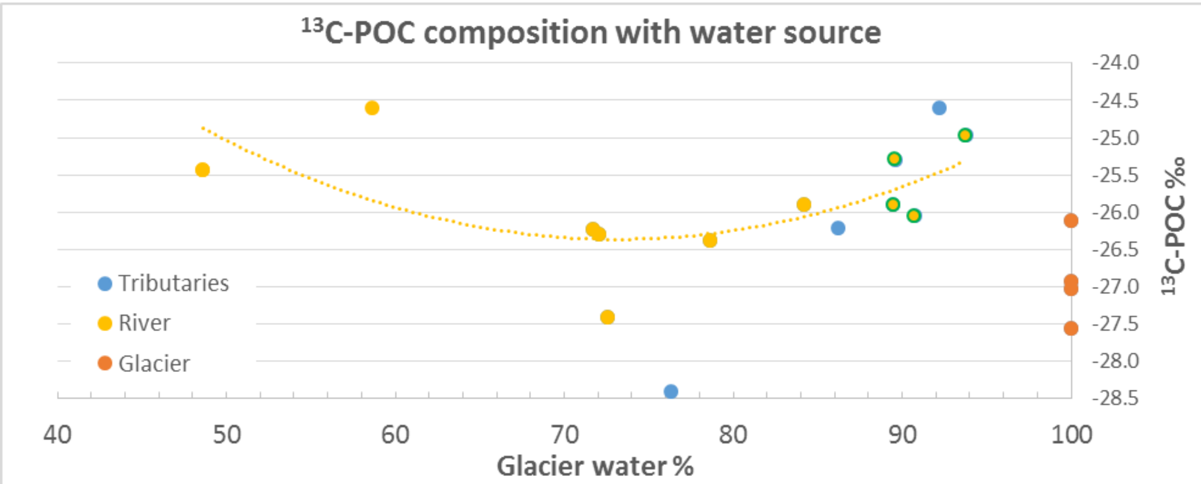

Figure 31; %glacier water plotted against δ13C-POC. River samples (yellow), tributaries (blue) and ice samples (orange) with in green circles the samples taken as a transect.

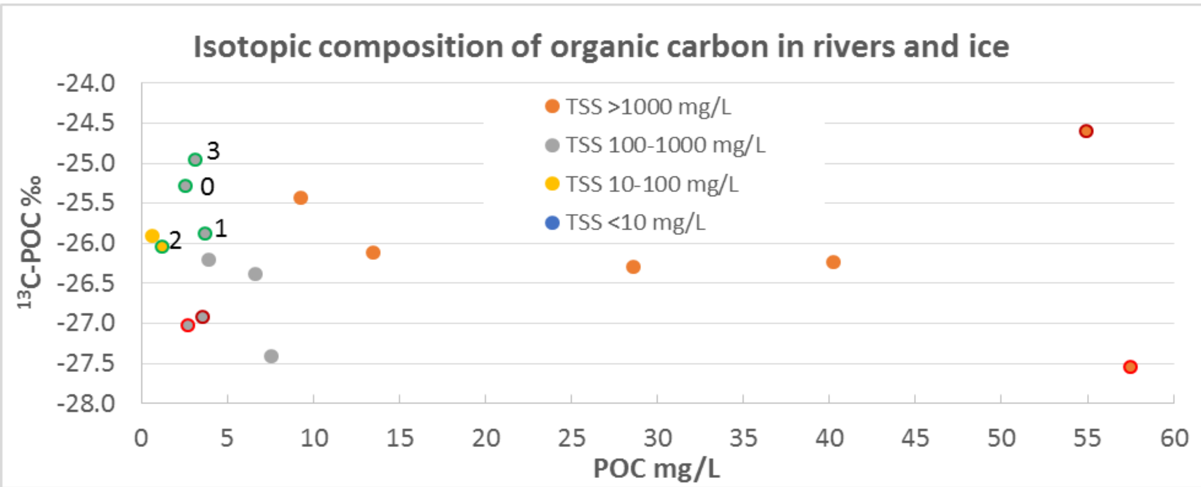

Figure 32; The isotopic composition and concentration of POC for ice (red circled) and river samples are plotted with the TSS values similar as in figure 30

4.3.3 Molecular analysis

The DOM has been analyzed by Fluorescence spectroscopy and FT-ICRMS for its molecular composition. The fluorescence data can distinguish mainly between humic versus protein-like structures. The FT-ICRMS can distinguish between molecular compounds and their masses (CHO (-N, -S, -NS)) together with the compound type such as aliphatics, phenols, aromatics and peptides. The data are visualized in EEMs for fluorescence and in graphs and tables for the FT-ICRMS data.

The EEMs from the fluorescence data are show in figure 33 and are placed in order from maximum to minimum percentage glacier-derived water in which the sample was taken. The letters in the plots are classified as follows:
*A and C: humic aromatics, mostly terrestrial from vascular plants
*M: humic and less aromatic than A and C, mostly microbial and often from marine/aquatic sources and in situ produced
*B and T: protein, mostly algal or microbial sources and is often a mixture of dissolved amino acids and other peptides.
*U: polycyclic aromatics, still mainly unknown but has been identified as from burned carbon

In the plots, the compounds A and M are most common, so most DOM is from humic and both terrestrial and microbial input. Compound C is found almost exclusively in larger rivers and not in ice samples, small tributaries or small glacier streams, and is probably picked up during transport to the ocean.
Compounds B and T show up randomly, but not when M, A or C is dominant. These protein structures are from microbial or algal sources. Since these compounds do not show up in every plot, they probably vary spatially. Peaks of compound B are found in different plots with no relationship to percentage glacier-derived water and with a change of a covariance with compound T. The ice samples are diverse, since there is no peak in the ice sample from Freemanbreen but there is one in the plot from the ice of Ulvebreen. Known is that ice contains highly spatial variable hotspot with algae and with just two samples no conclusion can be drawn from this. Other B and T peaks are from locations where snow melt could have played a role in the meltwater.

The relationship between the different compounds with percentage glacier-derived water is visualized in a principle component analysis (figure 34). Here, all variables are plotted and when two are found in the same quarter they covariate. The compounds as found by fluorescence agree with the EEM's plot, since both show is no covariation between percentage glacier-derived water and the compounds besides compound T. Compound T is not often present in DOM, so a one-to-one relationship is not significant in this data.

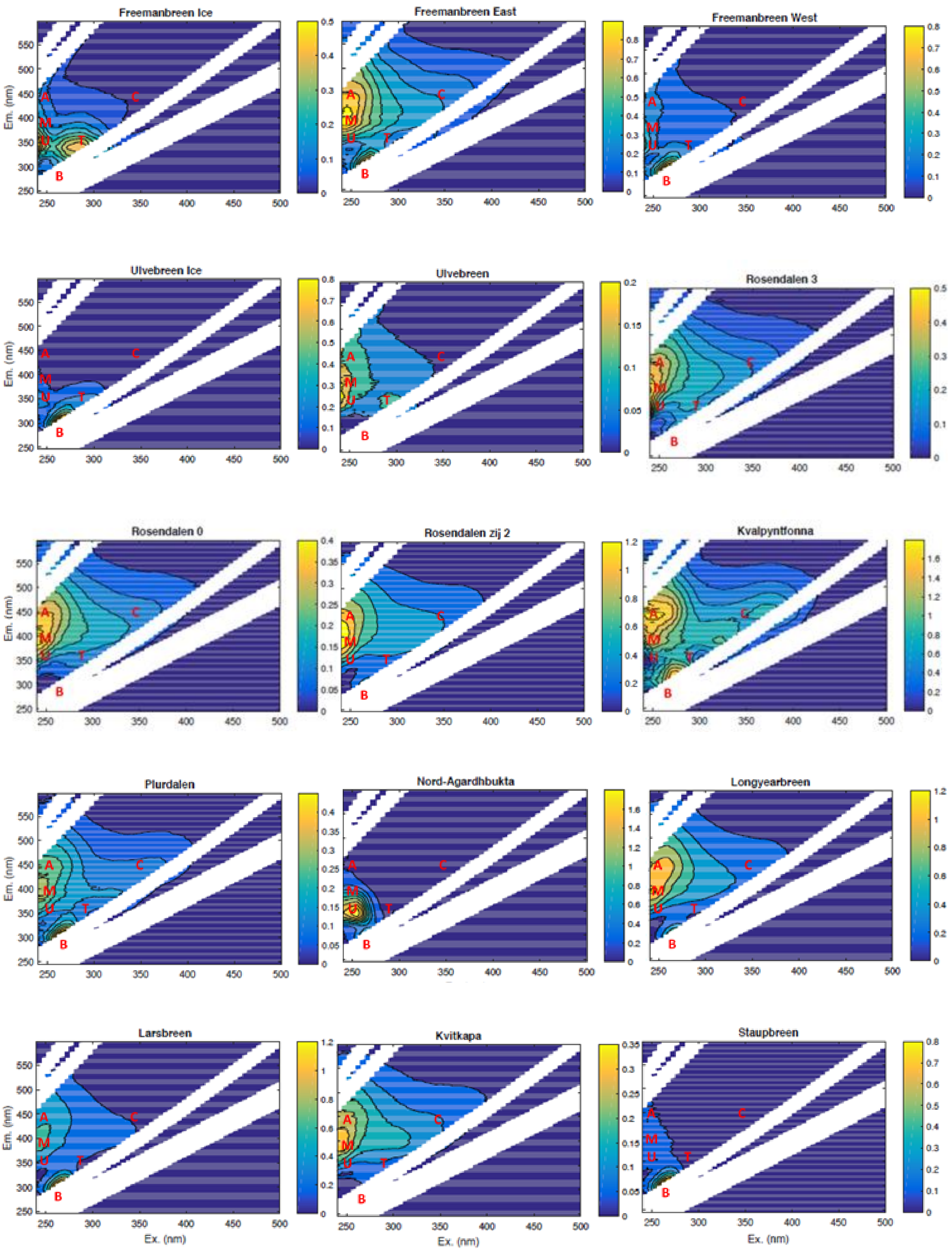

Figure 33; Fluorescence EEMs of different sample sites ordered from maximum glacial input (top left) to minimal glacial input (bottom right). Letters (red) show the assigned molecular characteristics (see text for specifications). The index is in Raman units.

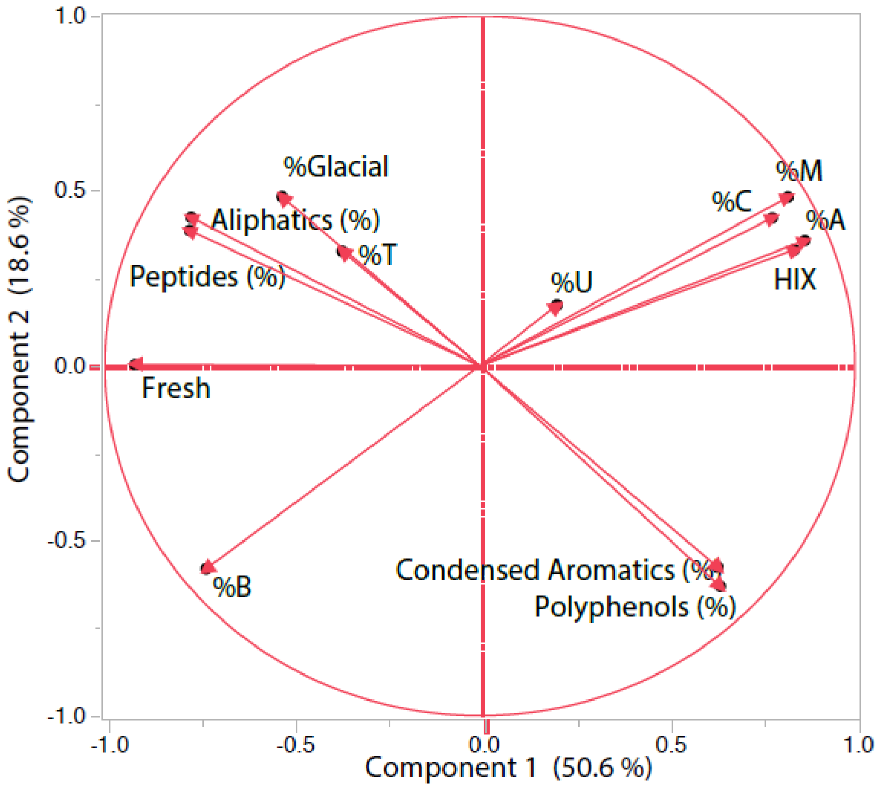

Figure 34; Principle component analysis of FT-ICRMS and Fluorescence data with percentage glacier-derived water. Data in the same quarter show covariance. Figure from A. Kellerman (Florida State University).

Table 9; The number and % of molecular formulas assigned to each defined compound class as measured by FT-ICRMS from total DOM. From top to bottom in order of percentage glacier-derived water.

Sample site	Condensed Aromatics	Polyphenols	Unsaturated Low Oxygen <0.5	Unsaturated High Oxygen >0.5	Aliphatics	Peptides
Freemanbreen East	1554 (9.82%)	2959 (18.7%)	5178 (32.7%)	3069 (19.4%)	1916 (12.1%)	1146 (7.42%)
Ulvebreen	467 (6.28%)	1110 (14.9%)	2716 (36.5%)	884 (11.9%)	1542 (20.7%)	722 (9.70%)
Ulvebreen ice	153 (5.58%)	374 (13.6%)	797 (29.1%)	372 (13.6%)	658 (24.0%)	387 (14.1%)
Rosendalen-3	292 (8.20%)	662 (18.6%)	1193 (33.5%)	704 (19.8%)	506 (14.2%)	204 (5.73%)
Rosendalen-0	1579 (9.75%)	3190 (19.7%)	5634 (34.8%)	2949 (18.2%)	1680 (10.4%)	1155 (7.14%)
Rosendalen-zij 2	848 (7.09%)	2052 (17.2%)	4611 (38.6%)	2667 (22.3%)	1344 (11.2%)	438 (3.66%)
Kvalpyntfonna	642 (7.42%)	1445 (16.7%)	2933 (33.9%)	1410 (16.3%)	1376 (15.9%)	846 (9.78%)
Plurdalen	688 (8.24%)	1370 (16.4%)	2280 (34.5%)	1834 (22.0%)	1302 (15.6%)	272 (3.26%)
Noord-Agardhbukta	498 (5.48%)	1367 (15.0%)	3083 (33.9%)	2075 (22.8%)	1442 (15.9%)	630 (6.93%)
Longyearbreen	1973 (14.5%)	3345 (24.6%)	4573 (33.6%)	2233 (16.4%)	1229 (9.03%)	257 (1.89%)
Larsbreen	1543 (11.0%)	3290 (23.4%)	4989 (35.5%)	2136 (15.2%)	1364 (9.72%)	714 (5.09%)
Kvitkapa	941 (9.57%)	1764 (17.9%)	3453 (35.1%)	2004 (20.4%)	1341 (13.6%)	333 (3.39%)

The data from the FT-ICRMS data on molecular structure and abundance are presented in table 9. Table 9 shows that condensed aromatics, also known as black carbons, are present in large number in all samples (5-15%). Black carbons are derived from forest fires and combustion of fossil fuels. Since forest fires do not occur in this region, the source will mainly be from Svalbard's mine companies and anthropogenic (fossil fuel) combusted aerosols. Highest numbers are found in water samples from Larsbreen and Longyearbreen, that are located in a populated area compared to the other samples. The only ice samples measured, from Ulvebreen, shows the lowest relative abundance of polyphenols and the highest number of aliphatics and peptides compared to the meltwater samples. Peptides are easily degraded, which can explain their decreasing abundance downstream. Also, polyphenols are derived from terrestrial material, and therefore expected more in larger rivers and further downstream.

The PCA (figure 34) underlines these findings, since covariation between percentages glacier-derived water and aliphatics and peptides is positive, and with polyphenols negative. The negative covariation with condensed aromatics is not assigned to percentage glacier-derived water but to a denser population in the area. To further investigate the relationships, the data are presented in a chart (figure 35). Here it is shown that these relationships have a weak significance and have a high variability.

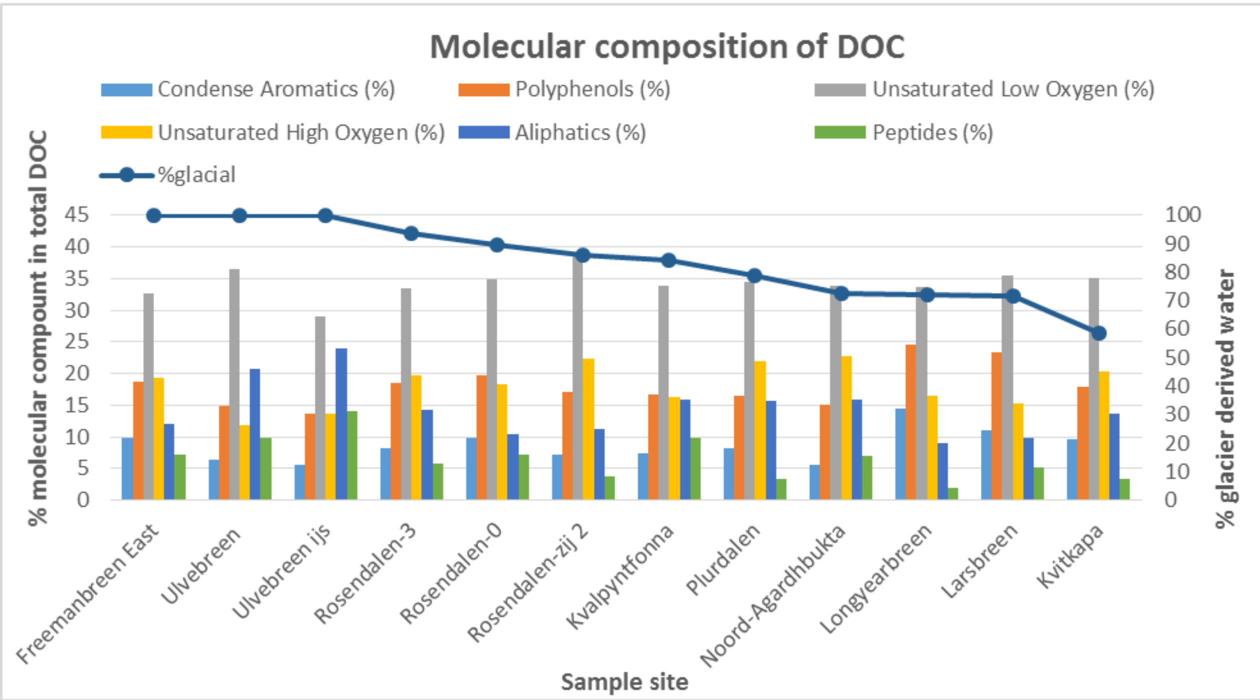

Figure 35; Graph of different molecular compound classes of DOM as measured by FT-ICRMS in percentages of the total DOM. In dark blue the percentage glacier-derived water per sample site.

5. Discussion

5.1 Glaciers

5.1.1 Volume estimation methods

To investigate the correlation of the volume/area scaling methods with the GIS method, the ice-volume results of all years (1971, 2004, 2014) and for all 4 ice caps have been plotted for both methods (figure 36). Figure 36 shows that the volume/area-scaling methods all have lower volume as derived by the GIS method. V/A-formulas closest the 1:1 relationship line are all from Radic&Hock (G1, G2, (Radić and Hock, 2010) with avgG closes to the 1:1 relationship. The avgG method is based on a combination of glacier and ice cap as arbitrary distinguished based on slope and perimeter. The average method, as a combination of all methods including the arbitrary distinghuised ice caps and glaciers shows an over underestimation for the v/a-scaling or overestimation of the GIS-method.

An overestimation of volume as derived by the GIS-method is more likely, since it's sensitive to the thickness of ice, calculated here with more uncertainty than the area as used in the V/A-scaling. The thickness of ice is based on Weertman's sliding law (Weertman, 1957) and depends on the equilibrium shear stress and the slope. The first is calculated by (Haeberli, 2005) for alpine regions based on the altitude difference in the glacier. Since the maximum altitude is hard to derive when the highest altitude is covered with an unknown thickness of ice, an offset of 100m would decrease the equilibrium shear stress with 16kPa leading to an overestimation of the ice thickness. Also, the slope is calculated based on the surface DEM. Most of the ice cap has a very flat ice surface, not per definition revealing the slope of the bed, which might be leading to an underestimation of the slope resulting in an overestimation of the ice thickness and therefore the ice caps volume. An overestimation of the ice thickness in the GIS-method is most likely the cause of its excess in calculated ice volume.

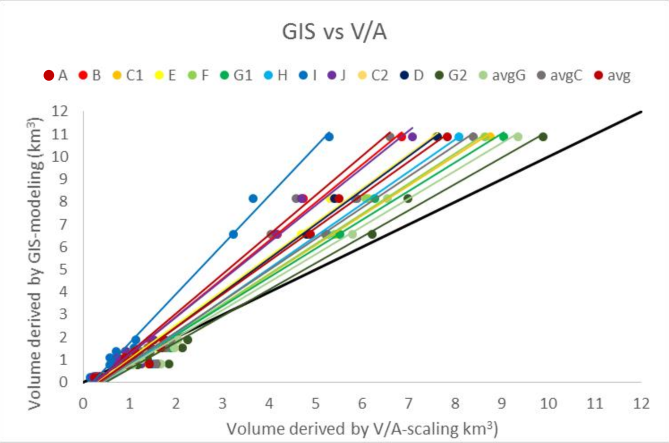

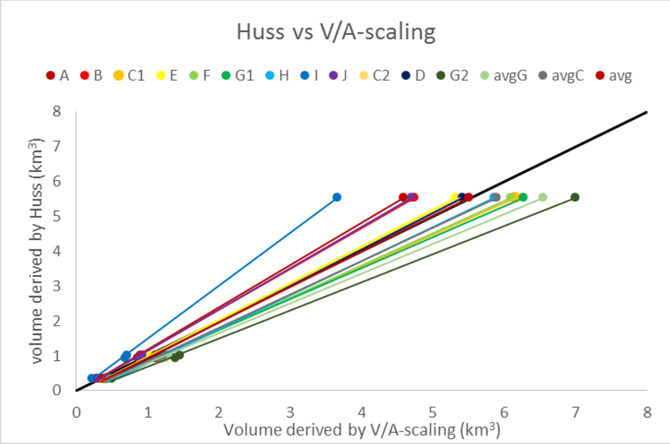

Figure 36; Correlation graphs between different methods. Trend lines are plotted between the calculated volumes per ice cap and per measurement year (1971, 2004 and 2014). The V/A-scaling results compared with the GIS-method (left) and Huss&Farinotti-method (right).

Huss&Farinotti's method corresponds very well with the V/A-scaling average and shows similar values as V/A-formulas E (Martín-Español et al., 2015) and H (Macheret and Zhuravlev, 1982), both were based on Svalbard's glaciers and D (Grinsted, 2013) which was derived for smaller glaciers. Similar as with the GIS-method, this method is based on ice flow. An important difference is the minimum slope, by Huss&Farinotti set at 6° degrees (1° in the GIS-method) and the use of Glen's flow law, which takes the thermal regime of the glacier and ice creep in account.

5.1.2 Mass balance and volume & area decline rate

Despite the volume difference derived by the different methods, both agree on a large decline in ice volume and area in 43 years, A: 40% V: 43.4±0.6% and A: 37% V: 42.6±3.1% for V/A-scaling and the GIS-method respectively, with larger losses for the smaller ice caps. The corresponding net mass balance is -0.93m/yr, which is increasing with time (-0.85m/yr for 1971-73 and -1.85m/yr for 2012-14). These values are larger then found in literature as previously described, for this area and much larger than estimates made for entire Svalbard, although reported estimation and observations are variable. Similar values found are by Nuth et al. (2013): they report a higher decline in Edgeøya and Barentsøya than in other regions in Svalbard with a mass loss of 18% in area from 1993 to 2000 compared to 7% for entire Svalbard. Kääb (2008) reports a mass loss of 17% and 25% for Digerfonna and Kvalpyntfonna, two ice caps at Edgeøya, from 1970-2002 with a mass balance of -0.55 and -0.61m/yr respectively. The acceleration in mass loss has also been reported in similar studies: James et al. (2012) found an increase in average thinning rate of 46% for Albrechtbreen at Edgeøya from 1961 to 2005 and -0.52m/yr prior to 1990 and -0.76m/yr after 1990 and on the rest of Svalbard (Bamber et al., 2005; James et al., 2012; Kääb, 2008; Kohler et al., 2007; Malecki, 2013). Since the surface area decreases, proportionally less volume would melt per year if the boundary conditions are kept constant. Although low, the V/A-scaling method does show a decrease in melt rate but the GIS-method an increase prior and after 2004, both indicating that the decline in ice volume is not linear but speeding up with present day warming.

The low values reported here might be an underestimation of the ice accumulation by precipitation. As in Hagen et al. (2003a), and Nowak and Hodson (2013) a precipitation correction per 100m altitude change with +20-30 and +19% per 100m respectively is used. If this would have been done for this research, the precipitation at 500m a.s.l. would have been doubled and the mass balance would have been less negative. On average this area receives 200mm precipitation per year. If we assume 20% extra precipitation per 100m altitude, at 300m a.s.l. a surplus of 145 mm/yr (0.145m) would have been added to precipitation, this would still keep the average net mass balance around -0.8m/yr (any influence on ice flux and albedo is not taken in account).

For the hydrology modelling, first the glacier's dynamics were modeled and calibrated until the area extent had the best fit with the glacier's area on the 2014 Landsat satellite images of August. The parameters were adjusted until the best fit was found. The DDF values are high (>14 mm/°C) and the temperature lapse rate low (<6°K/km) compared to similar research in other areas, but comparable values are found in previous reports about Svalbard (Claremar, 2013; Schytt, 1964).

Future projections for Svalbard glaciers as by Radić and Hock (2014) suggest a 55% loss in 2100. Here, with the assumption of the conservative value of 0.1 km^3/yr mass loss derived from V/A-scaling since '04, 100% of the ice mass (7.2 km^3) in Northwest Edgeøya will be gone prior to 2100. Projected increasing arctic atmospheric temperature (IPCC, 2013) not taken into account, which will be about +7°C at 2100, resulting in even faster ice mass decline rated than proposed here.

5.2 Hydrology

Hydrology has been modelled with the cryosphere-hydrology model of Immerzeel&Shea (Immerzeel et al., 2012; Shea et al., 2015), and due to lack of field data, not calibrated. Values used for the model set up have been calculated as explained. The graphs shown are used for comparison and relative change in time, and not for quantitative analyses.

The modelled annual total discharge shows 75% year to year variation and the annual average glacial discharge 48% variation. This is higher than the 30% reported in Svalbard glacier rivers on the island Spitsbergen (Hagen et al., 2003a) and the 40% reported after a modelling study by Radic et al. (2014). Also, the variation in both annual average discharge does not increase after 2000 as measured by Nowak and Hodson (2013) in Bayelva, Spitsbergen.

In the hydrographs, a decrease in peak flow is visible, but the baseflow and amount of days with glacier runoff do increase after mid-1990's elucidating an increase in glacier melt, revealing more moderate flow days. The shoulder month September is expected to be most vulnerable, since average temperature is near 0ºC (Nowak and Hodson, 2013). Here we do not report any change for the month September, and the more extreme precipitation events as expected in September (Nowak and Hodson, 2013; Xu et al., 2012) are not revealed in the precipitation data.

The discharge increases since the mid-1990's, as measured and modelled by many others (Bliss et al., 2014; Hagen et al., 2003a; Immerzeel et al., 2012; Nowak and Hodson, 2013; Radic et al., 2014), due to increased glacier melt. Since the glacier area is decreasing in size, more melt per unit area occurs. Expected is a decrease in melt when the area declines further, a process already visible in drainage area 5. The other areas only show no or a slight increase in glacial meltwater discharge, but all ice in these areas are thicker than as it is in area 5. In the modelled discharge 56% of the total discharge is on average from glacier melt, which is lower than reported by Hagen et al. (2003a) (67%) but similar as by Bliss et al. (2014) (51-68%).

The glacier melt contribution to total runoff does increase with time (figure 37) as a result of the increase in glacier melt. The 5-year moving average trend line shows a decline in runoff since 1995, after an initial increase in discharge. Whether this is due to internal variation or the onset of the decline in discharge due to glacier area decline as proposed by many, needs extra investigation. It does differ per drainage area in which most still show a slight increase, besides drainage area 5. That there is little change visible in annual discharge from 1971-2014 indicates that the extra melt per specific glacier area is increasing, since the area itself becomes smaller.

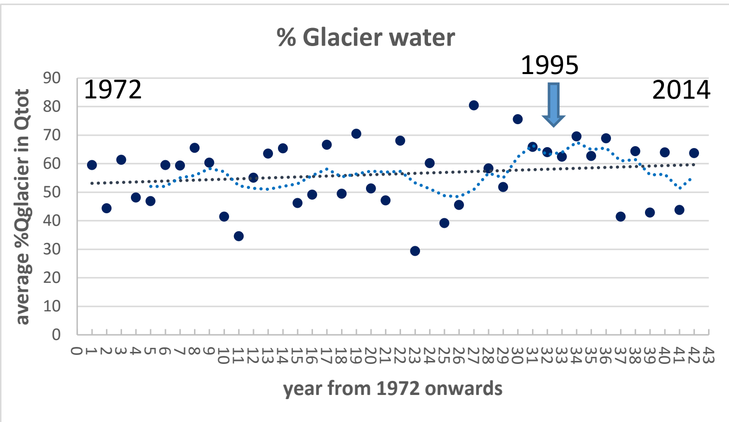

Figure 37; Percentage glacier-derived water in the total discharge as measured as sum of all outlet points for all drainage areas. Trend line is linear (dark) and a 5 year moving average (light).

5.3 Organic matter

The water isotopic composition corresponds with the LMWL, based on measurements on Spitsbergen, and has a slight d-excess for the melt water and ice samples. This can be explained by evaporation and refreezing enriching the δD and $\delta^{18}O$ of the residue water and ice (Yde et al., 2012).

The plot of $\delta^{13}C$-POC and %Glacier-derived water (figure 31) shows enrichment with more glacier water and enrichment with low percentage glacier water. Lighter $\delta^{13}C$-POC is expected in young, C3 plants (-25.5 to -29.3‰) and might be leaching from soils into the rivers (Kim et al., 2011) , and is therefore expected in water further from glaciers, which is also seen in figure 29. The enriched $\delta^{13}C$-POC can have two sources: microbial production in glaciers (Hood et al., 2009), which also might explain the lighter $\delta^{13}C$-POC with more glacier-derived water; and anthropogenic combustion products with enriched $\delta^{13}C$, brought by precipitation (Spencer et al., 2014a). A third method of enriching $\delta^{13}C$ is by photodegradation (Spencer et al., 2014b), which occurs in the Arctic but has not well studied yet.

The bioavailability (avg. 14±8%) and DOC values are very low (avg. 0.23±0.15 mg/L) compared to similar studies in Alaska, >40% and 0.18-0.53 mg/L, respectively (Fellman et al., 2010; Hood et al., 2009; Spencer et al., 2014a). This could be explained by the thin soil depth and low vegetation at Svalbard, compared to the Alaskan tundra, besides the incubation process in Alaska has been done with a marine inoculum instead of in situ bacteria.

TSS is dependent on discharge (Hudson and Ferguson, 1999) and the thermal regime of the glacier: warm based and polythermal glaciers transport more suspended sediments than cold based glaciers (Lapazaran et al., 2013). For Longyearbreen, previous research shows average values around 500-1000 mg/L with in August events of 6000 mg/L (Etzelmüller et al., 2000) our result is 5000mg/L in August, showing that the results can be highly variable, and that values here are a snapshot.

Both the fluorescence and FT-ICRMS data show highly variable results for molecular compounds measured in DOM in all water samples. Weak correlation is found between percentage glacier-derived water and aliphatics and peptides and a negative covariation with polyphenols. This is similar as described in (Hood et al., 2009), who found that glacier coverage had a positive relationship with percentage protein fluorescence in DOM in meltwater rivers. The negative covariation between condensed aromatics and percentage glacier-derived water is not assigned to source of water but to the relative population density of the area, since the highest percentages of black carbon are found near the (mine) town Longyearbyen. Differences in fluorescence between samples can likely be explained by greater processing or additional input during water transport (Spencer et al., 2014).

5.4 Synthesis

If we assume an average mass loss of 5.5 km^3 since 1971, which is 0.13 km^3/yr, than 4.0 m^3/s of the discharge is from glacier melt or 12.0 m^3/s if glacier melt is only be considered in the months June, July, August and September. The additional discharge is from precipitation and mass turn over. The POC and DOC carried in the water column are on average 12.1±16.9 and 0.23±0.15 mg/L respectively. This results in an additional OM transport to the ocean of 49.7 kg/s on an annual basis or 149 kg/s in the summer season, adding up to a total OM transport of 1.56 Mton/yr.

There are a few processes that are not fully considered in this study: Permafrost thaw can act as source of POC, DOC, and discharge, but it can also lead to increased water storage (Nowak and Hodson, 2013). Permafrost thaw increases with temperature, creating a potential water and OC source and sink for the future. Furthermore, we assume that all ice melt is considered to end as discharge to the ocean, and any refreezing and evapotranspiration is neglected. In the model this process is included, but the storage factor and groundwater recharge is too uncertain for this area, therefore qualitative numbers from meltwater modelling are not used here.

6. Conclusions

In this study different methods to determine ice volume loss have been used and implemented as initial state of a cryospheric hydrological model. The ice loss and meltwater fluxes have been combined with quantitative and qualitative organic matter analysis, to reveal source, flux and quality of organic carbon in a sensitive arctic ecosystem. The following conclusions can be drawn:

In 43 years (1971-2014) over 40% of glacier volume of NW Edgeøya's ice caps has been lost, with a conservative mass loss rate estimate of 0.12 km^3/yr. The GIS-method shows more positive values as the V/A-scaling and the method used by Huss&Farinotti, but still shows a negative projection for the future. If glacier loss continues with the same rate, prior to 2100 all ice will be lost, not taken any future warming projections in account.

The large mass loss leads to a decrease in peak flow, an increase in base flow, and increase in number of days with glacier melt, resulting in more days with moderate glacier runoff and an increase in %Qglacier in Qtot. For the future, a further decrease in discharge is expected due to glacier area loss, however, whether this is already occurring or still needs to happen is unclear. Field data of seasonal flow discharge to calibrate the model could elucidate this.

The DOC amount carried by these meltwater rivers is lower (0.23±0.15) and less bioavailable than in Alaska (Fellman et al., 2010; Hood et al., 2009; Spencer et al., 2014a). POC varies widely with on average 1.2% of transported TSS, which brings on average 12 ±16 mgC/L to the oceans. The source of the OC is mostly terrestrial matter (C3 plants with $\delta^{13}C$ -25 to -29‰) with input from ^{13}C-depleted englacial microbial production and/or anthropogenic combustion. The probability of anthropogenic combustion as source is strengthened by FT-ICRMS measurements in which black carbon can make up to 15% of total DOM in meltwater rivers.

Ice mass loss in northwestern Edgeøya since 1971 has brought 4,400,000,000,000 L of extra water to the oceans, carrying an extra 149 Kg C /s in the summer months than expected from discharge based on precipitation and mass turnover, which corresponds to 67Mton since 1971. Increasing temperature rise contributes to permafrost thaw, which is an extra source of POC, which can contribute to increasing C transport in the future. Decrease in mass loss rate, due to area loss, will decrease the discharge and likely also decrease the transport of OC to the oceans.

For reliable future projections more information is needed about seasonal discharge values and fluctuations, as well as about the source of the OC (permafrost thaw/erosion versus ice mass loss/combustion). Combined with OC degradation rates research in marine settings, this will give a better understanding of the sensitivity of the near shore coastal environment, which utilizes incoming glacial and terrestrial OC in their food web.

Acknowledgements

This master thesis would not have been this great without the help from a lot of people. First I would like to thank Dr. Jorien Vonk and Dr. Walter Immerzeel for supervision, but also for their open mind and degree of freedom I received to create an interdisciplinary master thesis. I am glad I had the opportunity to work on a subject I am really interested in and motivated for. Moreover, I want to thank Jorien as well for the financial support for the SEES expedition to Svalbard last summer. Also, I still had to learn some skills I missed during my master courses, so thank you Walter for giving me the opportunity to learn GIS and some basic modelling.

Then I want to thank Keechy for her labwork and together with Jessica, Jaco and Niels, they helped me to find motivation, creativity and developing new ideas during coffee breaks. Niels, Derek and Frits, thank you for your help with modelling, excel, and just general computer problems, without you I would still be copying and pasting single excel cells.

Last but not least, special thanks to all who read my thesis, to improve my English, help with understanding the fluvial system and to help with the setup of the whole thesis, Alphons, Robert and Thomas.

References

Anesio, A. M., Hodson, A. J., Fritz, A., Psenner, R. and Sattler, B.: High microbial activity on glaciers: Importance to the global carbon cycle, Glob. Chang. Biol., 15(4), 955–960, doi:10.1111/j.1365-2486.2008.01758.x, 2009.

Bahr, D. B., Meier, M. F. and Peckham, S. D.: The physical basis of glacier volume-area scaling, J. Geophys. Res., 102(B9), 20355, doi:10.1029/97JB01696, 1997.

Bamber, J., Krabill, W., Raper, V., Dowdeswell, J. and Oerlemans, J.: Elevation change measured on Svalbard glaciers and ice caps from airborne laser data, Ann. Glaciol., 42, 202–208, 2005.

Bliss, A., Hock, R. and Radić, V.: Global response of glacier runoff to twenty-first century climate change, J. Geophys. Res. Earth Surf., 119(4), 717–730, doi:10.1002/2013JF002931, 2014.

Braithwaite, R. J. and Raper, S. C. B.: Glaciological conditions in seven contrasting regions estimated with the degree-day model, Ann. Glaciol., 46(2002), 297–302, doi:10.3189/172756407782871206, 2007.

Chen, J. and Ohmura, A.: Estimation of Alpine glacier water resources and their change since the 1870's, Hydrol. Mt. Reg. I, 193, 1990.

Claremar, B.: Relation between meso-scale climate and glacier / snow mass balance on Svalbard, SVALI Deliv. Rep. D2.3-11, 2013.

Dowdeswell, J. a and Bamber, J. L.: On the glaciology of Edgeoya and Barentsoya , Svalbard, Polar Res., 14(2), 105 – 122, 1995.

Etzelmüller, B., Ødegård, R. S., Vatne, G., Mysterud, R. S., Tonning, T. and Sollid, J. L.: Glacier characteristics and sediment transfer system of Longyearbreen and Larsbreen, western Spitsbergen, Nor. Geogr. Tidsskr. - Nor. J. Geogr., 54(4), 157–168, doi:10.1080/002919500448530, 2000.

Fellman, J. B., Spencer, R. G. M., Hernes, P. J., Edwards, R. T., D'Amore, D. V. and Hood, E.: The impact of glacier runoff on the biodegradability and biochemical composition of terrigenous dissolved organic matter in near-shore marine ecosystems, Mar. Chem., 121(1-4), 112–122, doi:10.1016/j.marchem.2010.03.009, 2010.

Glen, J. W.: The Creep of Polycrystalline Ice, Proc. R. Soc. London A Math. Phys. Eng. Sci., 228(1175), 519–538 [online] Available from: http://rspa.royalsocietypublishing.org/content/228/1175/519.abstract, 1955.

Grinsted, a.: An estimate of global glacier volume, Cryosphere, 7(1), 141–151, doi:10.5194/tc-7-141-2013, 2013.

Haeberli, W.: Investigating glacier-permafrost relationships in high-mountain areas: historical background, selected examples and research needs, Geol. Soc. London, Spec. Publ., 242(1), 29–37, doi:10.1144/GSL.SP.2005.242.01.03, 2005.

Hagen, J. O., Lefauconnier, B. and Liestol, O.: Glacier mass balance in Svalbard since 1912, Glaciers-ocean-atmosph. Interact. Proc. Symp. St. Petersburg, 1990, 313–328 [online] Available from: http://www.scopus.com/inward/record.url?eid=2-s2.0-0026291323&partnerID=tZOtx3y1, 1991.

Hagen, J. O., Kohler, J., Melvold, K. and Winther, J. G.: Glaciers in Svalbard: Mass balance, runoff and freshwater flux, Polar Res., 22(2), 145–159, doi:10.1111/j.1751-8369.2003.tb00104.x, 2003a.

Hagen, J. O., Melvold, K., Pinglot, F. and Dowdeswell, J. A.: On the Net Mass Balance of the Glaciers and Ice Caps in Svalbard, Norwegian Arctic, Arctic, Antarct. Alp. Res., 35(2), 264–270, doi:10.1657/1523-0430(2003)035[0264:OTNMBO]2.0.CO;2, 2003b.

Hood, E., Fellman, J., Spencer, R. G. M., Hernes, P. J., Edwards, R., D'Amore, D. and Scott, D.: Glaciers as a source of ancient and labile organic matter to the marine environment., Nature, 462(7276), 1044–1047, doi:10.1038/nature08580, 2009.

Hood, E., Battin, T. J., Fellman, J., O'Neel, S. and Spencer, R. G. M.: Glaciers Storage and release of organic carbon from glaciers and ice sheets, Nat. Geosci., (January), doi:10.1038/ngeo2331, 2015.

Hudson, A. J. and Ferguson, R. I.: Fluvial suspended sediment transport from cold and warm-based glaciers in Svalbard, Earth Surf. Process. Landforms, 24(11), 957–974, doi:10.1002/(SICI)1096-9837(199910)24:11<957::AID-ESP19>3.0.CO;2-J, 1999.

Huss, M. and Farinotti, D.: Distributed ice thickness and volume of all glaciers around the globe, J. Geophys. Res. Earth Surf., 117(4), 1–10, doi:10.1029/2012JF002523, 2012.

Immerzeel, W. W., van Beek, L. P. H., Konz, M., Shrestha, a. B. and Bierkens, M. F. P.: Hydrological response to climate change in a glacierized catchment in the Himalayas, Clim. Change, 110(3-4), 721–736, doi:10.1007/s10584-011-0143-4, 2012.

Immerzeel, W. W., Pellicciotti, F. and Bierkens, M. F. P.: Rising river flows throughout the twenty-first century in two Himalayan glacierized watersheds, Nat. Geosci., 6(9), 742–745, doi:10.1038/ngeo1896, 2013.

James, T. D., Murray, T., Barrand, N. E., Sykes, H. J., Fox, a. J. and King, M. a.: Observations of enhanced thinning in the upper reaches of Svalbard glaciers, Cryosph., 6(6), 1369–1381, doi:10.5194/tc-6-1369-2012, 2012.

Jiyang Chen and Ohmura, A.: Estimation of Alpine glacier water resources and their change since the 1870s, Hydrol. Mt. Reg. I, 127–135 [online] Available from: http://www.scopus.com/inward/record.url?eid=2-s2.0-0025584970&partnerID=tZOtx3y1, 1990.

Kääb, a.: Glacier volume changes using ASTER sattelite stereo and ICESat GLAS Laser Altimetry. A test study on Edgeoya, eastern Svalbard, IEEE Trans. Geosci. Remote Sens., 46(10), 2823–2830, 2008.

Kane, D. L., Soden, D. J., Hinzman, L. D. and Gieck, R. E.: Rainfall runoff of a nested watershed in the alaskan arctic, , (55), 539–544, 1998.

Karssenberg, D., Törnqvist, T. E. and Bridge, J. S.: Conditioning a process-based model of sedimentary architecture to well data, J. Sediment. Res., 71(6), 868–879, doi:1527-1404/01/071-868, 2001.

Kim, J.-H., Peterse, F., Willmott, V., Kristensen, D. K., Baas, M., Schouten, S. and Sinninghe Damsté, J. S.: Large ancient organic matter contributions to Arctic marine sediments (Svalbard), Limnol. Oceanogr., 56(4), 1463–1474, doi:10.4319/lo.2011.56.4.1463, 2011.

Kohler, J., James, T. D., Murray, T., Nuth, C., Brandt, O., Barrand, N. E., Aas, H. F. and Luckman, a.: Acceleration in thinning rate on western Svalbard glaciers, Geophys. Res. Lett., 34(18), 1–5, doi:10.1029/2007GL030681, 2007.

Lapazaran, J., Petlicki, M. and Navarro, F.: Ice volume changes (1936-1990-2007) and ground-penetrating radar studies of Ariebreen, Hornsund, Spitsbergen, Polar Res., c, 1–10 [online] Available from: http://www.polarresearch.net/index.php/polar/article/view/11068, 2013.

Macheret, Y. Y. and Zhuravlev, a B.: Radio echo soundings of Svalbard glaciers, J. Glaciol., 28(99), 295–314, 1982.

Malecki, J.: Elevation and volume changes of seven Dickson Land glaciers, Svalbard, 1960-1990-2009, Polar Res., 32(18400), 1–12, doi:http://dxdoi.org/10.3402/polar.v32i0.18400, 2013.

Mann, P. J., Eglinton, T. I., McIntyre, C. P., Zimov, N., Davydova, A., Vonk, J. E., Holmes, R. M. and Spencer, R. G. M.: Utilization of ancient permafrost carbon in headwaters of Arctic fluvial networks., Nat. Commun., 6, 7856, doi:10.1038/ncomms8856, 2015.

Marshall, A. G., Hendrickson, C. L. and Jackson, G. S.: Fourier transform ion cyclotron resonance mass spectrometry: a primer., Mass Spectrom. Rev., 17(1), 1–35, doi:10.1002/(SICI)1098-2787(1998)17:1<1::AID-MAS1>3.0.CO;2-K, 1998.

Martín-Español, a., Navarro, F. J., Otero, J., Lapazaran, J. J. and Błaszczyk, M.: Estimate of the total volume of Svalbard glaciers, and their potential contribution to sea-level rise, using new regionally based scaling relationships, J. Glaciol., 61(225), 29–41, doi:10.3189/2015JoG14J159, 2015.

Martin-Espanol, A.: Estimate of the total ice volume of svalbard glaciers and their potential contribution to sea-level rise, phD thesis, 2013.

Moholdt, G., Nuth, C., Hagen, J. O. and Kohler, J.: Recent elevation changes of Svalbard glaciers derived from ICESat laser altimetry, Remote Sens. Environ., 114(11), 2756–2767, doi:10.1016/j.rse.2010.06.008, 2010.

Moller, P., Stubdrup, O. P. and Kronborg, C.: Late Weichselian to early Holocene sedimentation in a steep fjord/valley setting, Visdalen, Edgeoya, eastern Svalbard: glacial deposits, alluvial/colluvial-fan deltas and spit-platforms, Polar Res., 14(2), 181–203, doi:10.1111/j.1751-8369.1995.tb00688.x, 1995.

Mosher, J. J., Kaplan, L. A., Podgorski, D. C., McKenna, A. M. and Marshall, A. G.: Longitudinal shifts in dissolved organic matter chemogeography and chemodiversity within headwater streams: a river continuum reprise, Biogeochemistry, 124(1-3), 371–385, doi:10.1007/s10533-015-0103-6, 2015.

Nowak, A. and Hodson, A.: Hydrological response of a High-Arctic catchment to changing climate over the past 35 years: A case study of Bayelva watershed, Svalbard, Polar Res., 32(1), 1–16, doi:10.3402/polar.v32i0.19691, 2013.

Nuth, C., Moholdt, G., Kohler, J., Hagen, J. O. and Kääb, A.: Svalbard glacier elevation changes and contribution to sea level rise, J. Geophys. Res. Earth Surf., 115(1), 1–16, doi:10.1029/2008JF001223, 2010.

Nuth, C., Kohler, J., König, M., Von Deschwanden, a., Hagen, J. O., Kääb, a., Moholdt, G. and Pettersson, R.: Decadal changes from a multi-temporal glacier inventory of Svalbard, Cryosphere, 7(5), 1603–1621, doi:10.5194/tc-7-1603-2013, 2013.

Oerlemans, J., Giesen, R. H. and Van Den Broeke, M. R.: Retreating alpine glaciers: Increased melt rates due to accumulation of dust (Vadret da Morteratsch, Switzerland, J. Glaciol., 55(192), 729–736, doi:10.3189/002214309789470969, 2009.

Osterkamp, T. E. and Burn, C. R.: Permafrost., 2003.

Owczarek, P., Nawrot, A., Migala, K., Malik, I. and Korabiewski, B.: Flood-plain responses to contemporary climate change in small High-Arctic basins (Svalbard, Norway), Boreas, 43(2), 384–402, doi:10.1111/bor.12061, 2014.

Radic, V., Bliss, A., Cody, A. B., Hock, R., Miles, E. and Cogley, J. G.: Regional and global projections of twenty-first century glacier mass changes in response to climate scenarios from global climate models, Clim. Dyn., 42, 37–58, 2014.

Radić, V. and Hock, R.: Regional and global volumes of glaciers derived from statistical upscaling of glacier inventory data, J. Geophys. Res. Earth Surf., 115(1), 1–10, doi:10.1029/2009JF001373, 2010.

Radić, V. and Hock, R.: Glaciers in the Earth's Hydrological Cycle: Assessments of Glacier Mass and Runoff Changes on Global and Regional Scales, Surv. Geophys., doi:10.1007/s10712-013-9262-y, 2014.

Rutter, N., Hodson, A., Irvine-Fynn, T. and Solås, M. K.: Hydrology and hydrochemistry of a deglaciating high-Arctic catchment, Svalbard, J. Hydrol., 410(1-2), 39–50, doi:10.1016/j.jhydrol.2011.09.001, 2011.

Schytt, V.: Scientific results of the Swedish Glaciologogical expedition to Nordaustlandet, Spitsbergen, 1957 and 1958, , 46(3), 242–282, 1964.

Shea, J. M., Immerzeel, W. W., Wagnon, P., Vincent, C. and Bajracharya, S.: Modelling glacier change in the Everest region , Nepal Himalaya, Cryosph., 9, 1105–1128, doi:10.5194/tc-9-1105-2015, 2015.

Sobota, I.: Selected methods in mass balance estimation of Waldemar Glacier, Spitsbergen, Polish Polar Res., 28(4), 249–268, 2007.

Van Soelen, E. E., Lammers, J. M., Eglinton, T. I., Sinninghe Damsté, J. S. and Reichart, G. J.: Unusual C35 to C38 alkenones in mid-Holocene sediments from a restricted estuary (Charlotte Harbor, Florida), Org. Geochem., 70, 20–28, doi:10.1016/j.orggeochem.2014.01.021, 2014.

Spencer, R. G. M., Vermilyea, A., Fellman, J., Raymond, P., Stubbins, A., Scott, D. and Hood, E.: Seasonal variability of organic matter composition in an Alaskan glacier outflow: insights into glacier carbon sources, Environ. Res. Lett., 9(5), 055005, doi:10.1088/1748-9326/9/5/055005, 2014a.

Spencer, R. G. M., Guo, W., Raymond, P. a., Dittmar, T., Hood, E., Fellman, J. and Stubbins, A.: Source and biolability of ancient dissolved organic matter in glacier and lake ecosystems on the Tibetan Plateau, Geochim. Cosmochim. Acta, 142, 64–74, doi:10.1016/j.gca.2014.08.006, 2014b.

Spencer, R. G. M., Mann, P. J., Dittmar, T., Eglinton, T. I., Mcintyre, C., Holmes, R. M., Zimov, N. and Stubbins, A.: Detecting the signature of permafrost thaw in Arctic rivers, Geophys. Res. Lett., 42, 1–6, doi:10.1002/2015GL063498.Received, 2015.

Stubbins, A. and Dittmar, T.: Low volume quantification of dissolved organic carbon and dissolved nitrogen, Limnol. Oceanogr. Methods, 10, 347–352, doi:10.4319/lom.2012.10.347, 2012.

Svendsen, J. I. and Mangerud, J.: Holocene glacial and climatic variations on Spitsbergen, Svalbard, The Holocene, 7(1), 45–57, 1997.

Turner, K. W., Wolfe, B. B. and Edwards, T. W. D.: Characterizing the role of hydrological processes on lake water balances in the Old Crow Flats, Yukon Territory, Canada, using water isotope tracers, J. Hydrol., 386(1-4), 103–117, doi:10.1016/j.jhydrol.2010.03.012, 2010.

Vonk, J. E., Mann, P. J., Davydov, S., Davydova, A., Spencer, R. G. M., Schade, J., Sobczak, W. V., Zimov, N., Zimov, S., Bulygina, E., Eglinton, T. I. and Holmes, R. M.: High biolability of ancient permafrost carbon upon thaw, Geophys. Res. Lett., 40(11), 2689–2693, doi:10.1002/grl.50348, 2013.

Van De Wal, R. S. W. and Wild, M.: Modelling the response of glaciers to climate change by applying volume-area scalling in combination with a high resolution GCM, Clim. Dyn., 18(3-4), 359–366, doi:10.1007/s003820100184, 2001.

Weertman, J.: On the sliding of glaciers, J. Glaciol., 3, 33–38, doi:10.1007/978-94-015-8705-1_19, 1957.

Westermann, S., Langer, M. and Boike, J.: Spatial and temporal variations of summer surface temperatures of high-arctic tundra on Svalbard - Implications for MODIS LST based permafrost monitoring, Remote Sens. Environ., 115(3), 908–922, doi:10.1016/j.rse.2010.11.018, 2011.

Xu, M., Yan, M., Kang, J. and Ren, J.: Comparative studies of glacier mass balance and their climatic implications in Svalbard, Northern Scandinavia, and Southern Norway, Environ. Earth Sci., 67(5), 1407–1414, doi:10.1007/s12665-012-1585-3, 2012.

Yde, J. C., Hodson, A. J., Solovjanova, I., Steffensen, J. P., Nørnberg, P., Heinemeier, J. and Olsen, J.: Chemical and isotopic characteristics of a glacier-derived naled in front of Austre Grønfjordbreen, Svalbard, Polar Res., 31(0), 1–15, doi:10.3402/polar.v31i0.17628, 2012.

Yi, Y., Gibson, J. J., Cooper, L. W., Hélie, J.-F., Birks, S. J., McClelland, J. W., Holmes, R. M. and Peterson, B. J.: Isotopic signals (^{18}O, ^{2}H, ^{3}H) of six major rivers draining the pan-Arctic watershed, Global Biogeochem. Cycles, 26(1), n/a–n/a, doi:10.1029/2011GB004159, 2012.